Supporting information for:

Electronic Traps and Phase Segregation in Lead Mixed-Halide Perovskite

Alexander J. Knight, Adam D. Wright, Jay B. Patel, David P. McMeekin, Henry J. Snaith, Michael B. Johnston, and Laura M. Herz*

University of Oxford

E-mail: laura.herz@physics.ox.ac.uk

Contents

1 Sample Fabrication

Substrate cleaning: z-cut quartz was first cleaned using Hellmanex, acetone and isopropanol, then with oxygen plasma for 10 minutes.

MAPb($Br_{0.5}I_{0.5}$)$_3$ perovskite layer preparation: The MAPb($Br_{0.5}I_{0.5}$)$_3$ perovskite was prepared using an adaptation procedure proposed by F. Huang *et al.*[S1] The perovskite films were prepared by dissolving the precursor salts in anhydrous N,N-dimethylformamide (DMF) and dimethyl sulfoxide (DMSO) mixture (4:1 volume ratio) to obtain a stoichiometric solution with the desired MAPb($Br_{0.5}I_{0.5}$)$_3$ composition. The precursor solution was prepared using the following precursor salts: formamidinium iodide (FAI) (dyesol), formamidinium bromide (FABr) (dyesol), lead iodide (PbI_2) (99%, Sigma-Aldrich), lead bromide ($PbBr_2$) (98%, Alfa Aesar). The perovskite precursor solution was spin coated from a 1.0 M solution at 4000 rpm for 30 seconds. N_2 gas was used to quench the growth of the perovskite. The gas flow was applied 15 seconds after the start of the spin coating, and sustained for 10 seconds. The perovskite films were immediately placed on a preheated hot plate set to 100 °C and annealed in a N_2 atmosphere for 20 minutes.

Poly(methyl methacrylate) (PMMA) layer preparation: PMMA (Sigma Aldrich, average M_W 97,000) was dissolved in chlorobenzene with a concentration of 150 mg mL^{-1}. The solution was spin coated at 2000 rpm for 45 seconds on top of the perovskite films.

Final sample preparation: The back of the quartz substrate was cleaned with isopropanol to ensure no residue at the back of the sample would interfere with measurements.

2 Sample Characterization

Sample Thickness: The thickness of the MAPb($Br_{0.5}I_{0.5}$)$_3$ (MA = $CH_3NH_3^+$) perovskite and poly(methyl methacrylate) (PMMA) layers of the samples was measured from SEM cross-sectional images (see Figure S1). The average perovskite layer thickness was found to be 390 nm ± 12% and the average PMMA layer thickness to be 1300 nm ± 6%.

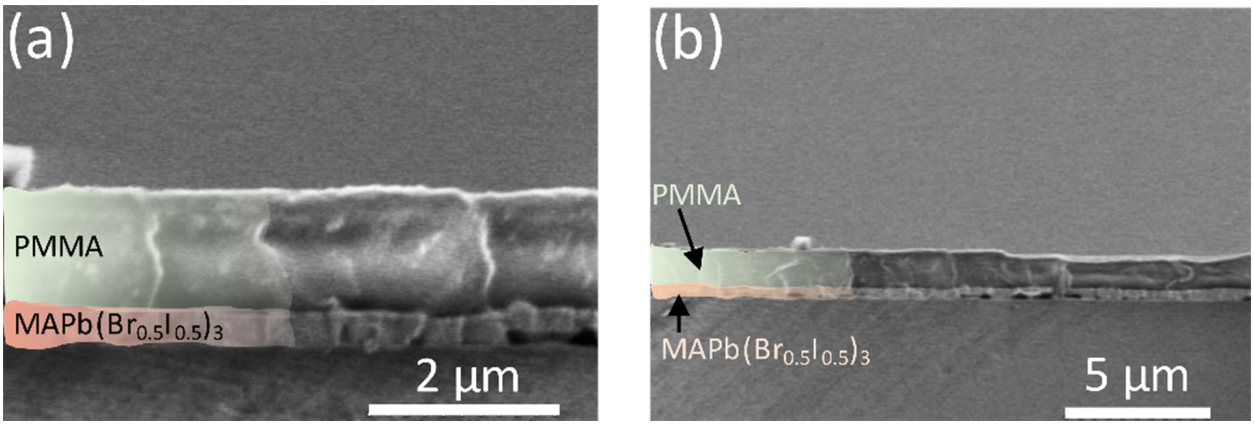

Figure S1: Cross-sectional SEM images of the $MAPb(Br_{0.5}I_{0.5})_3$ films with the poly(methyl methacrylate) (PMMA) coating. The same section of film is shown in (a) with a scalebar of 2 µm and in (b) with a scalebar of 5 µm.

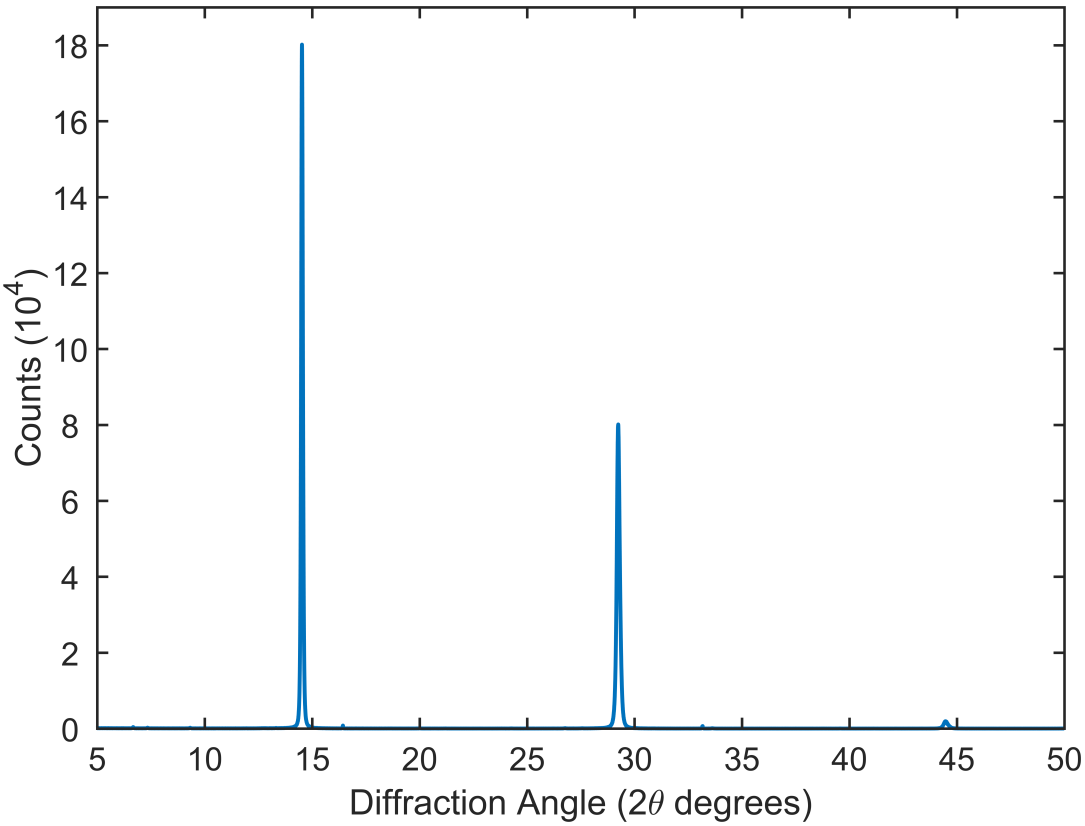

Figure S2: XRD pattern taken from a $MAPb(Br_{0.5}I_{0.5})_3$ film coated with a thick layer of poly(methyl methacrylate) (PMMA).

X-Ray Diffraction (XRD) Measurement: An XRD pattern was obtained from the same $MAPb(Br_{0.5}I_{0.5})_3$ films coated with a thick layer of poly(methyl methacrylate) (PMMA)

used in the various experiments reported here and in the main text (other than the specified samples in the atmospheric experiment presented in Figure 1 and Section S4). The XRD pattern was taken from diffraction angle 2θ =5° to 50° at a scan speed of $0.015\,^{\circ}\,s^{-1}$ and obtained with a PANalytical X'Pert Powder X-Ray Diffractometer. The Cu-K_α line was used as incident radiation. In order to correct against sample tilt, the z-cut quartz peak in the data was used as a reference and fixed to 2θ =16.43°.

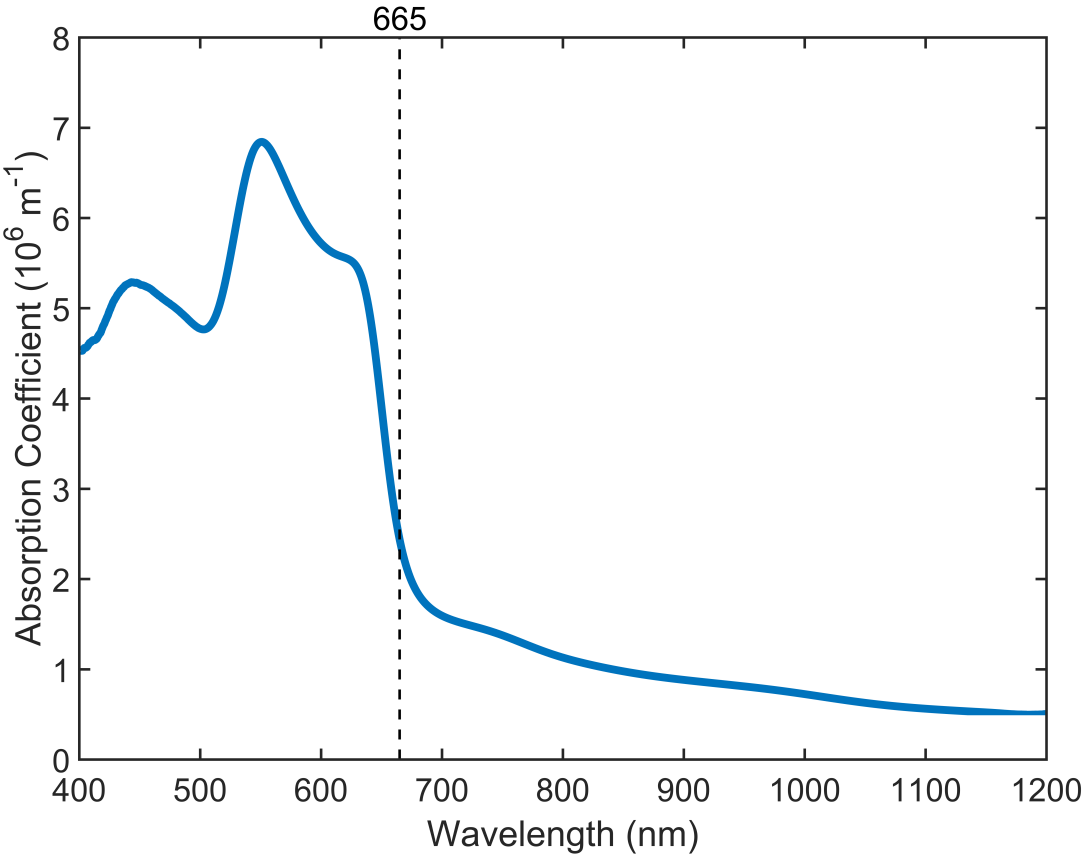

Figure S3: Absorption spectrum of a $MAPb(Br_{0.5}I_{0.5})_3$ film coated with a thick layer of poly(methyl methacrylate) (PMMA).

Absorption Spectrum Measurement: An absorption spectrum was obtained from the same $MAPb(Br_{0.5}I_{0.5})_3$ films coated with a thick layer of poly(methyl methacrylate) (PMMA) used in the various experiments reported here and in the main text (other than the specified samples in the atmospheric experiment presented in Figure 1 and Section S4). The measurements were conducted with a Bruker Vertex 80v Fourier-transform infrared spectrometer

fitted with the reflection/transmission accessory, a tungsten halogen lamp source, a CaF beamsplitter, and a silicon diode detector. The reflectance reference spectrum was performed on a Thorlabs UV-protected silver mirror, and the transmission reference spectrum was performed on a clean quatrz substrate.

3 Calculations of the AM1.5-Equivalent Excitation Intensity

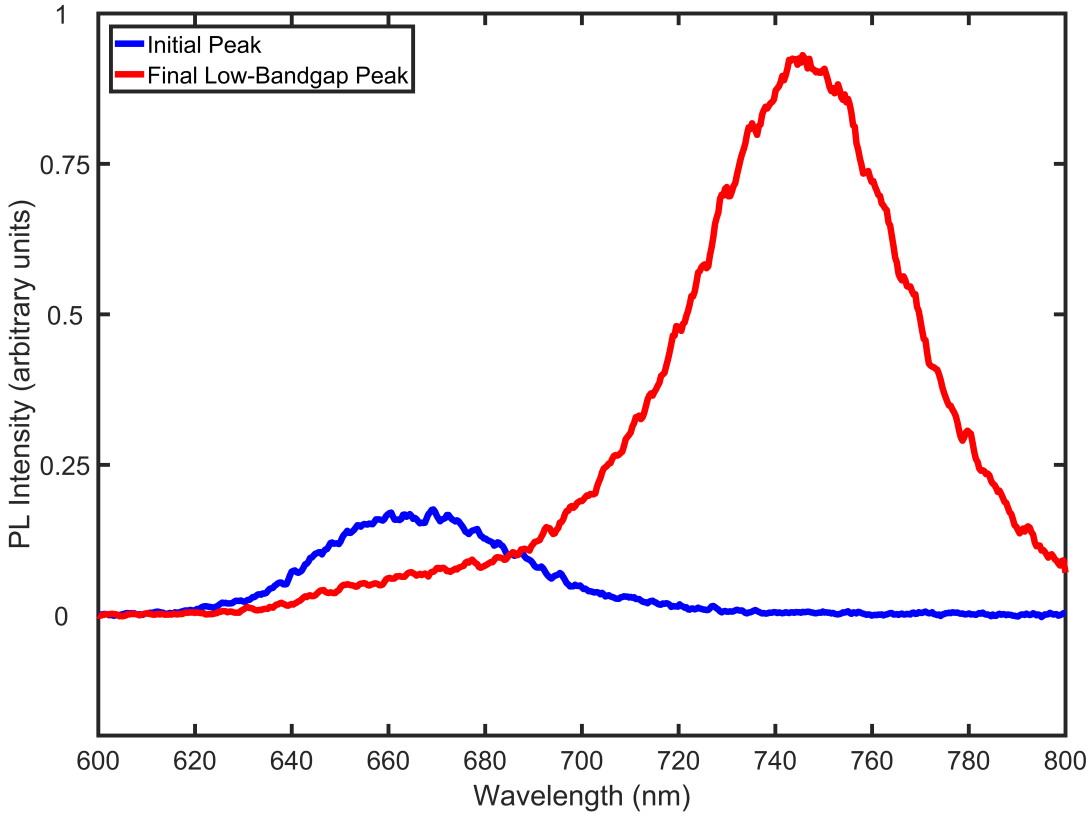

Figure S4: The wavelength of the emitted light from PMMA coated samples held under vacuum before (blue) and after (red) 21 seconds of light-soaking under 4.1 kW m^{-2} intensity illumination at 400 nm wavelength. The emission wavelength of the initial PL peak was determined to be 665 nm and the wavelength of the formed, low-bandgap PL peak varied across spots on the perovskite films, but was generally measured around 745 nm.

We define "AM1.5 equivalent intensity" as the laser intensity at which the same density

of charge carriers is photoexcited in the perovskite film as would be under the AM1.5 solar spectrum.[S2] Due to the sharp absorption onset in our perovskite films (Figure S3) we expect only a small number of above-gap photons to pass through the entire film, and thus in our calculations we assume total absorption of all incident photons with energies higher than the bandgap. The AM1.5 equivalent intensity is therefore taken to be the same laser intensity at which the flux of incident laser photons matches the flux of above-bandgap photons from the AM1.5 spectrum. The bandgap of the mixed-phase perovskite was determined to be around 665 nm from measurements of the PL and absorption spectra (Figures S4 and S3 respectively), while the iodide-rich phase produced an emissive peak centered on different values depending on the measurement taken, likely due to spot-to-spot variations in the perovskite films. The formed iodide-rich phase PL peak was also observed to red-shift as the perovskite film segregated further, thus making the determination of a bandgap for the iodide-rich perovskite difficult. 745 nm was determined as a suitable representative value, as highlighted by the red curve in Figure S4. Calculating the effective bandgap of a segregating material is complicated, however it has been reported that the majority of the perovskite remains near the initial stoichiometric composition throughout the segregation process, with only around 20% of the perovskite converting to the iodide-rich phase.[S3] Hence for our calculation of an AM1.5 equivalent intensity we selected an effective bandgap of 680 nm as a 80:20 weighted average of the mixed and iodide-rich perovskite bandgaps. While no single effective bandgap can be completely accurate at all times as the film segregates, our defined laser intensity should generate the same order of magnitude of charge carriers in our films as the AM1.5 spectrum would. The AM1.5 Spectrum represents the power per unit area emitted from the sun at different photon wavelengths, denoted here as AM1.5(λ)[S2] and measured in $\mathrm{W\,m^{-2}\,nm^{-1}}$. The number of photons emitted per unit time in the wavelength range λ to $\lambda + \mathrm{d}\lambda$ is then $\mathrm{AM1.5}(\lambda) \times (\frac{hc}{\lambda})^{-1} \times \mathrm{d}\lambda$, where $\frac{hc}{\lambda}$ is the energy of a photon with a wavelength of λ. Integrating over this expression from $\lambda = 0\,\mathrm{nm}$ to $\lambda = 680\,\mathrm{nm}$ reveals that there are 1.19×10^{21} photons per second per meter squared above bandgap incident on our

material under an AM1.5 spectrum for the given scenario. The value of 1.19×10^{21} photons per second per meter squared at 400 nm wavelength then corresponds to a laser power of $591\,\mathrm{W\,m^{-2}}$, which is taken as our AM1.5 equivalent power.

In addition, the generation rate of photoexcited charge carriers within our films under the AM1.5 spectrum is calculated from the photon flux. The generation rate is assumed to be spatially independent as the photoexcited charge carriers quickly spread through the film's depth profile through charge carrier diffusion and photon-recycling processes.[S4] Hence a value of 1.19×10^{21} charge carriers per second per meter squared above bandgap spread evenly through a 390 nm thick film corresponds to a generation rate of $3.05 \times 10^{27}\,\mathrm{m^{-3}\,s^{-1}}$, or $3.05 \times 10^{21}\,\mathrm{cm^{-3}\,s^{-1}}$, which is also, by definition, the expected generation rate under our laser at AM1.5 equivalent intensity.

4 Halide Segregation Under Different Atmospheres

In order to test the influence of the atmospheric composition on halide segregation, $MAPb(Br_{0.5}I_{0.5})_3$ perovskite films with and without a protective layer of poly(methyl methacrylate) (PMMA) coating were exposed to repeated cycles of illumination and darkness under different atmospheres: vacuum at a pressure of around 0.2 mbar, air at atmospheric pressure, and nitrogen at a pressure of around 2 bar. No difference was seen in the data depending on whether samples were illuminated from either side of the films. Halide segregation was induced by illumination of the films with a continuous wave, 400 nm wavelength diode laser (Picoharp, LDH-D-C-405M) at AM1.5 equivalent intensity (see Section S3) for 15 seconds, over which 5 short measurements were taken. To complete a cycle, the films were then left to relax in darkness for 30 minutes – much longer than the illumination time – as it has been observed that the halide segregation rate is faster than the ion remixing rate in similar films.[S3] This illumination/darkness cycle was then repeated 8 times as part of an experimental run. The same spot was always illuminated within an experimental run,

and between experimental runs a fresh spot that had not yet been illuminated was always selected under darkness. The photoluminescence (PL) from the sample was collected and coupled into a grating spectrometer (Princeton Instruments, SP-2558), where the light was dispersed by its wavelength and detected by an iCCD camera (PI-MAX4, Princeton Instruments). The intensity of the light emerging from the mixed-phase and iodide-rich perovskite regions was determined by integration over the two associated spectral regions, at around 640 nm to 690 nm and 720 nm to 770 nm, respectively. The PL intensities from the samples under different environmental conditions and from both spectral regions are plotted in Figures S5-S13.

In order to create Figure 1 in the main paper, each experimental run was normalized such that the initial measurement of the mixed-phase perovskite PL intensity was set to 1. The data from similar atmospheric conditions was then averaged, and the standard deviation calculated. These statistics are plotted in Figure 1 in the main paper.

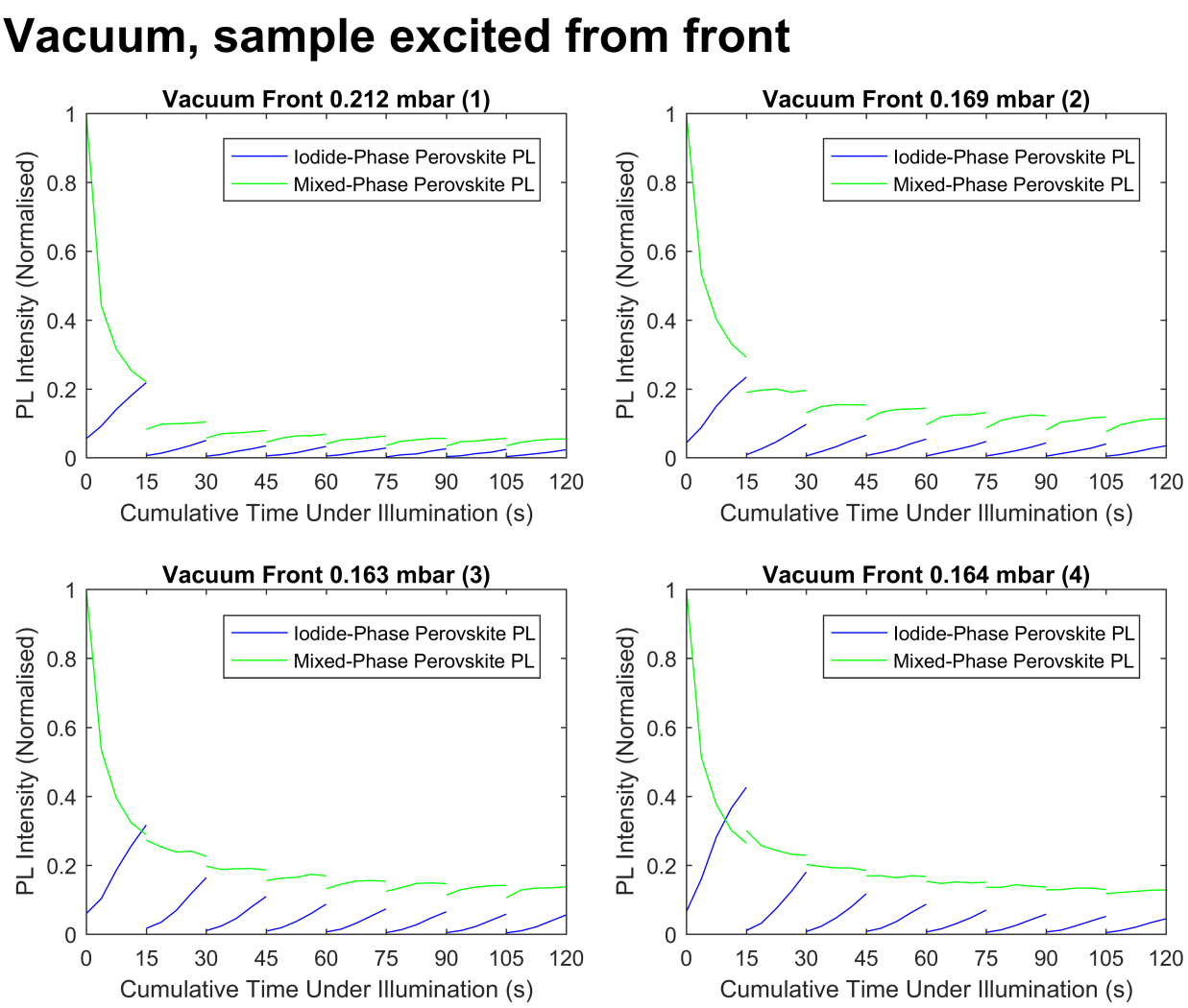

Figure S5: PL data highlighting the reversibility of halide segregation when $MAPb(Br_{0.5}I_{0.5})_3$ films are held under vacuum and illuminated from the front (the film side). To induce repeated segregation and remixing, the films were exposed to 8 illumination cycles, with a single cycle consisting of 15 seconds of illumination followed by 30 minutes of darkness. Illumination was achieved with a 400 nm wavelength laser at AM1.5 equivalent power (see Section S3). The blue lines show the integrated intensity of the iodide-rich phase PL peak (around 720 nm to 770 nm) and the green lines the integrated intensity of the mixed-halide phase PL peak (around 640 nm to 690 nm), both normalized such that the initial mixed-phase measurement is set to 1.

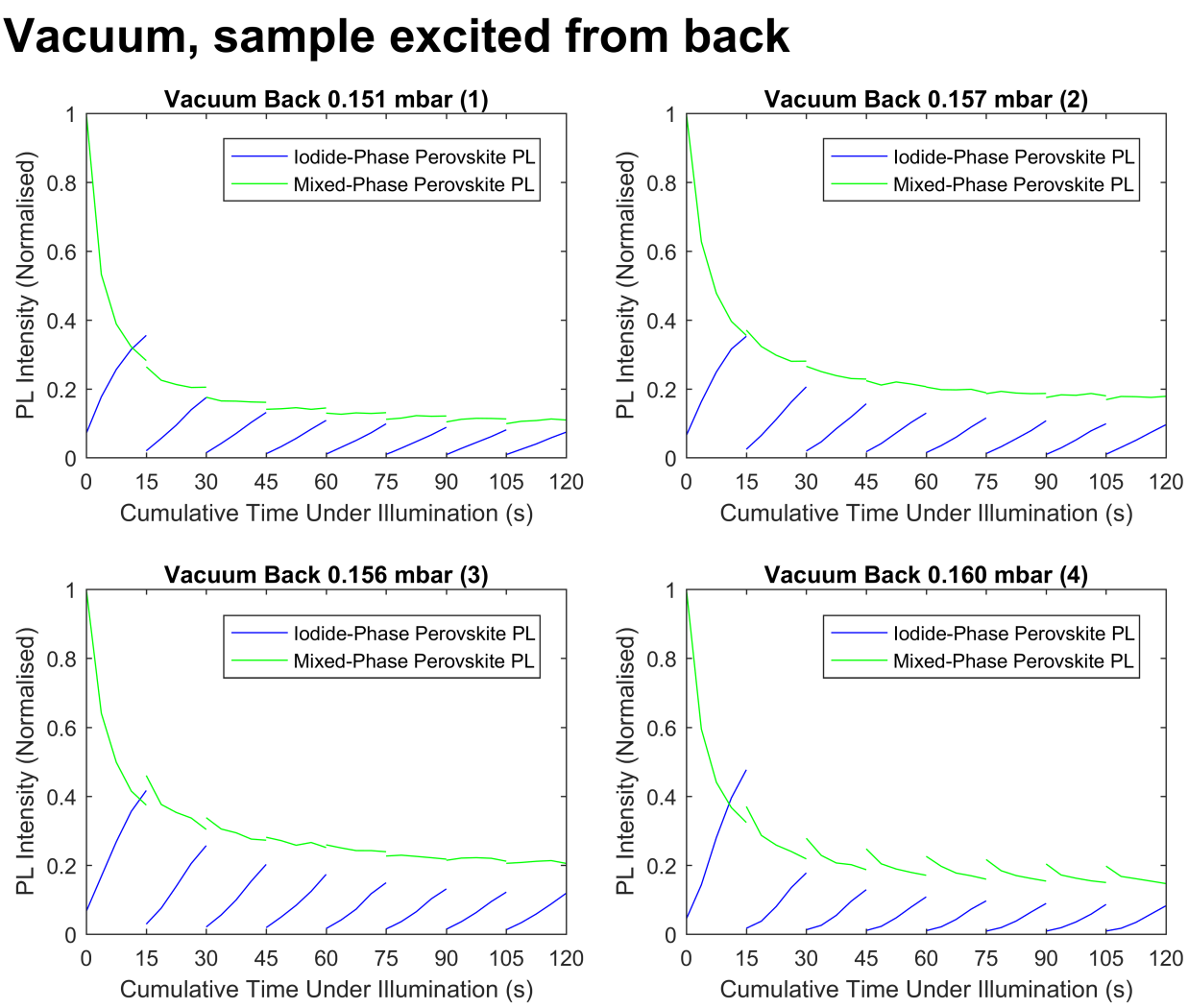

Figure S6: PL data highlighting the reversibility of halide segregation when $MAPb(Br_{0.5}I_{0.5})_3$ films are held under vacuum and illuminated from the back (the substrate side). To induce repeated segregation and remixing, the films were exposed to 8 illumination cycles, with a single cycle consisting of 15 seconds of illumination followed by 30 minutes of darkness. Illumination was achieved with a 400 nm wavelength laser at AM1.5 equivalent power (see Section S3). The blue lines show the integrated intensity of the iodide-rich phase PL peak (around 720 nm to 770 nm) and the green lines the integrated intensity of the mixed-halide phase PL peak (around 640 nm to 690 nm), both normalized such that the initial mixed-phase measurement is set to 1.

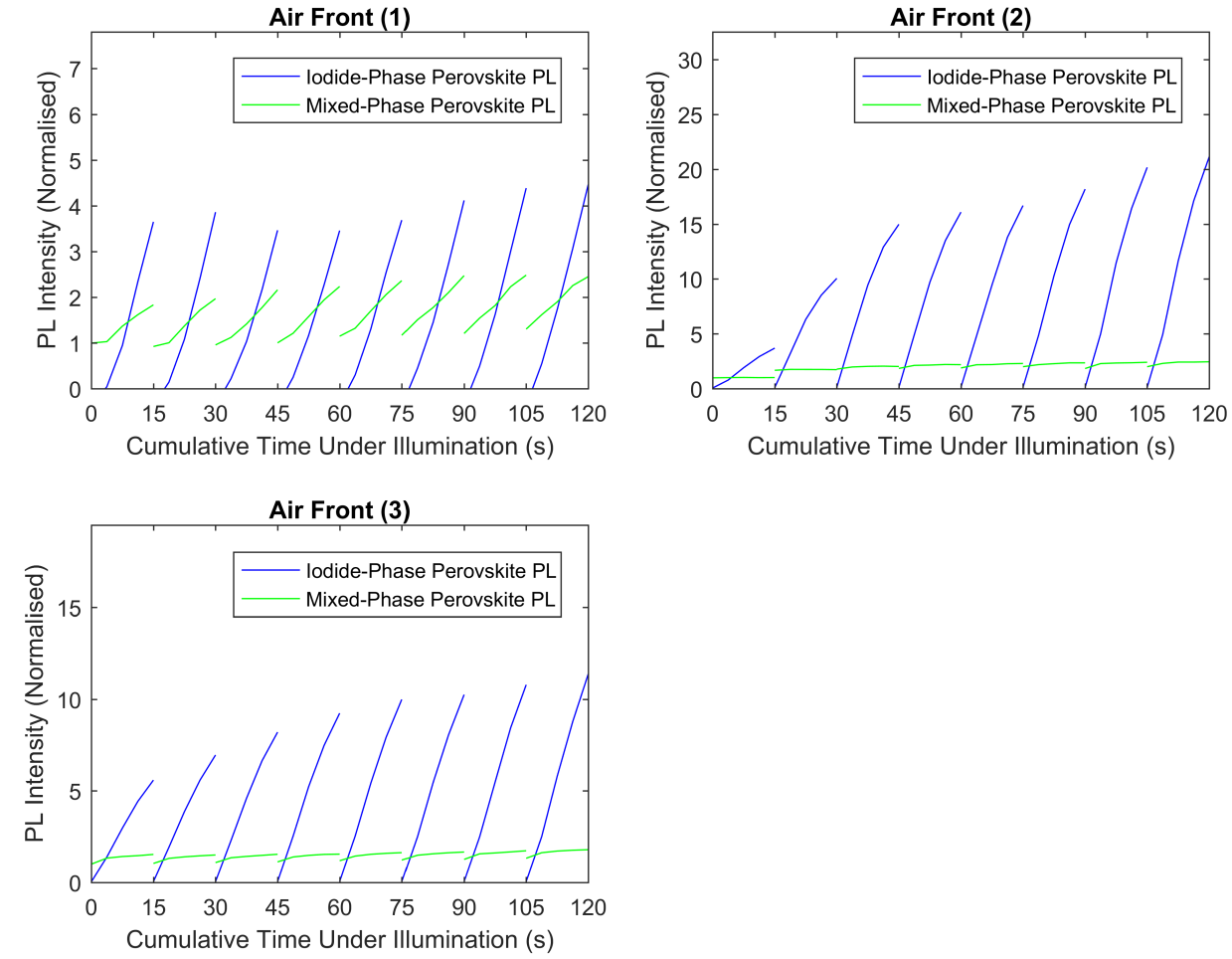

Figure S7: PL data highlighting the reversibility of halide segregation when $MAPb(Br_{0.5}I_{0.5})_3$ films are held under air and illuminated from the front (the film side). To induce repeated segregation and remixing, the films were exposed to 8 illumination cycles, with a single cycle consisting of 15 seconds of illumination followed by 30 minutes of darkness. Illumination was achieved with a 400 nm wavelength laser at AM1.5 equivalent power (see Section S3). The blue lines show the integrated intensity of the iodide-rich phase PL peak (around 720 nm to 770 nm) and the green lines the integrated intensity of the mixed-halide phase PL peak (around 640 nm to 690 nm), both normalized such that the initial mixed-phase measurement is set to 1.

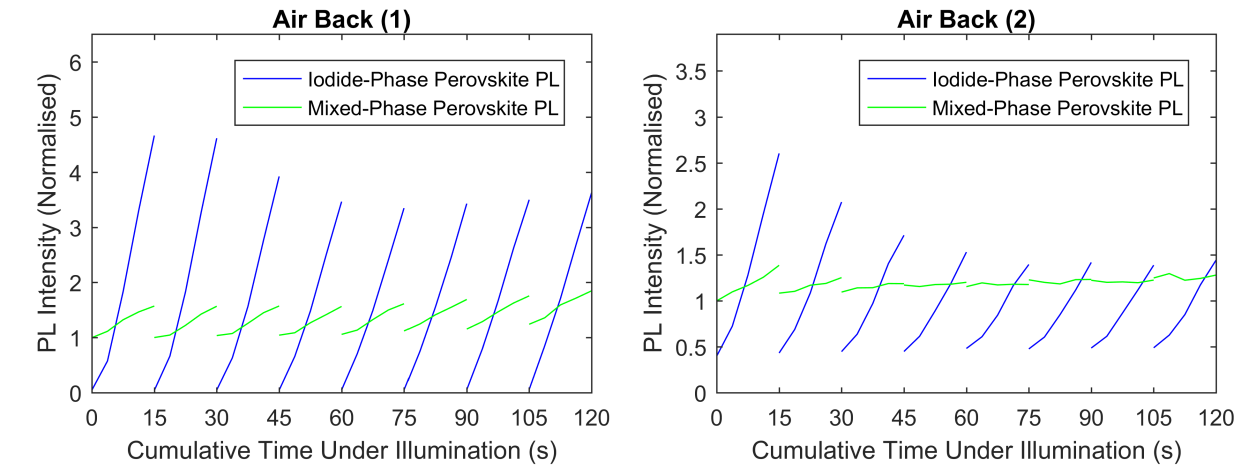

Figure S8: PL data highlighting the reversibility of halide segregation when $MAPb(Br_{0.5}I_{0.5})_3$ films are held under air and illuminated from the back (the substrate side). To induce repeated segregation and remixing, the films were exposed to 8 illumination cycles, with a single cycle consisting of 15 seconds of illumination followed by 30 minutes of darkness. Illumination was achieved with a 400 nm wavelength laser at AM1.5 equivalent power (see Section S3). The blue lines show the integrated intensity of the iodide-rich phase PL peak (around 720 nm to 770 nm) and the green lines the integrated intensity of the mixed-halide phase PL peak (around 640 nm to 690 nm), both normalized such that the initial mixed-phase measurement is set to 1.

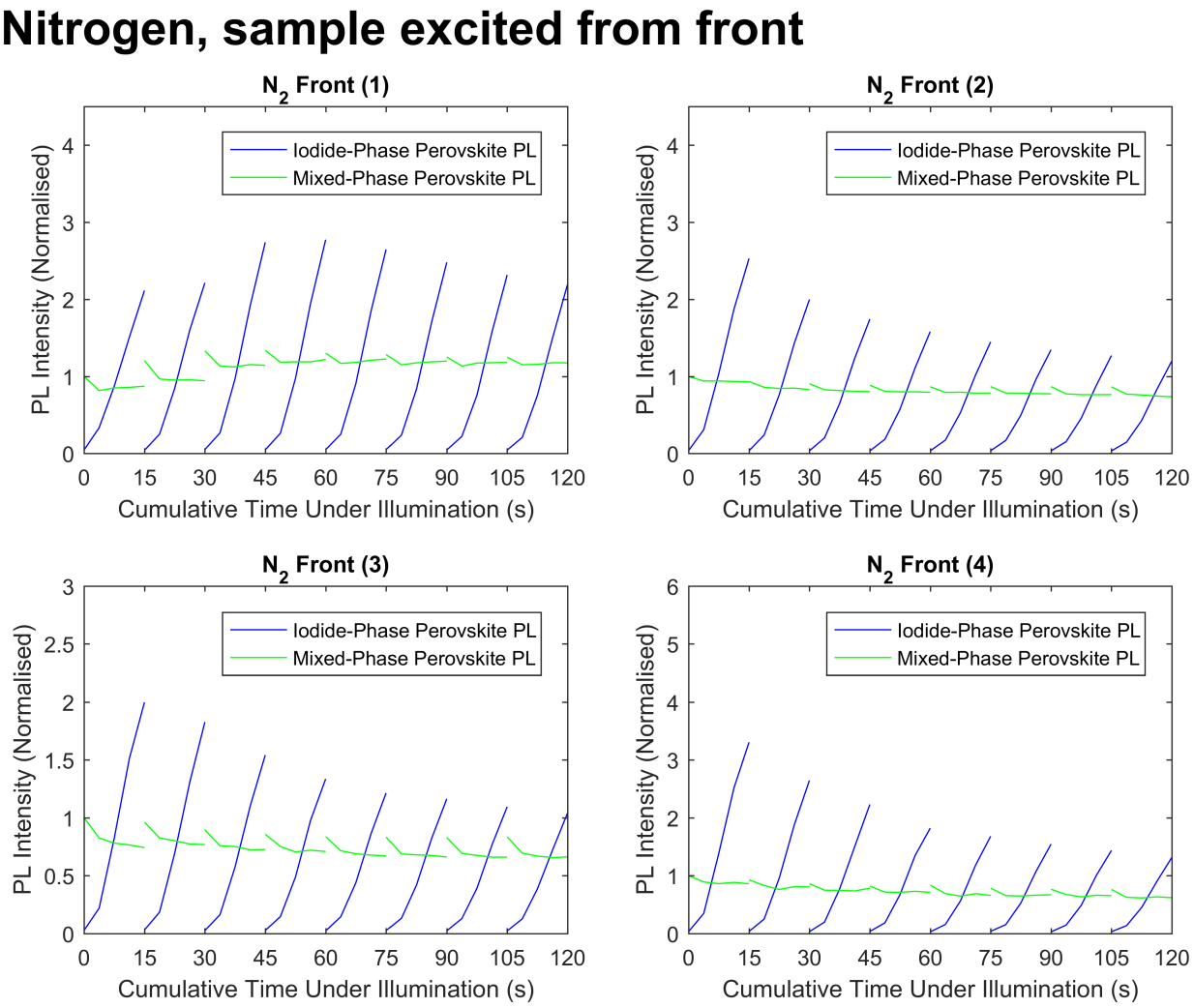

Figure S9: PL data highlighting the reversibility of halide segregation when $MAPb(Br_{0.5}I_{0.5})_3$ films are held under pressurized nitrogen (around 2 bar) and illuminated from the front (the film side). To induce repeated segregation and remixing, the films were exposed to 8 illumination cycles, with a single cycle consisting of 15 seconds of illumination followed by 30 minutes of darkness. Illumination was achieved with a 400 nm wavelength laser at AM1.5 equivalent power (see Section S3). The blue lines show the integrated intensity of the iodide-rich phase PL peak (around 720 nm to 770 nm) and the green lines the integrated intensity of the mixed-halide phase PL peak (around 640 nm to 690 nm), both normalized such that the initial mixed-phase measurement is set to 1.

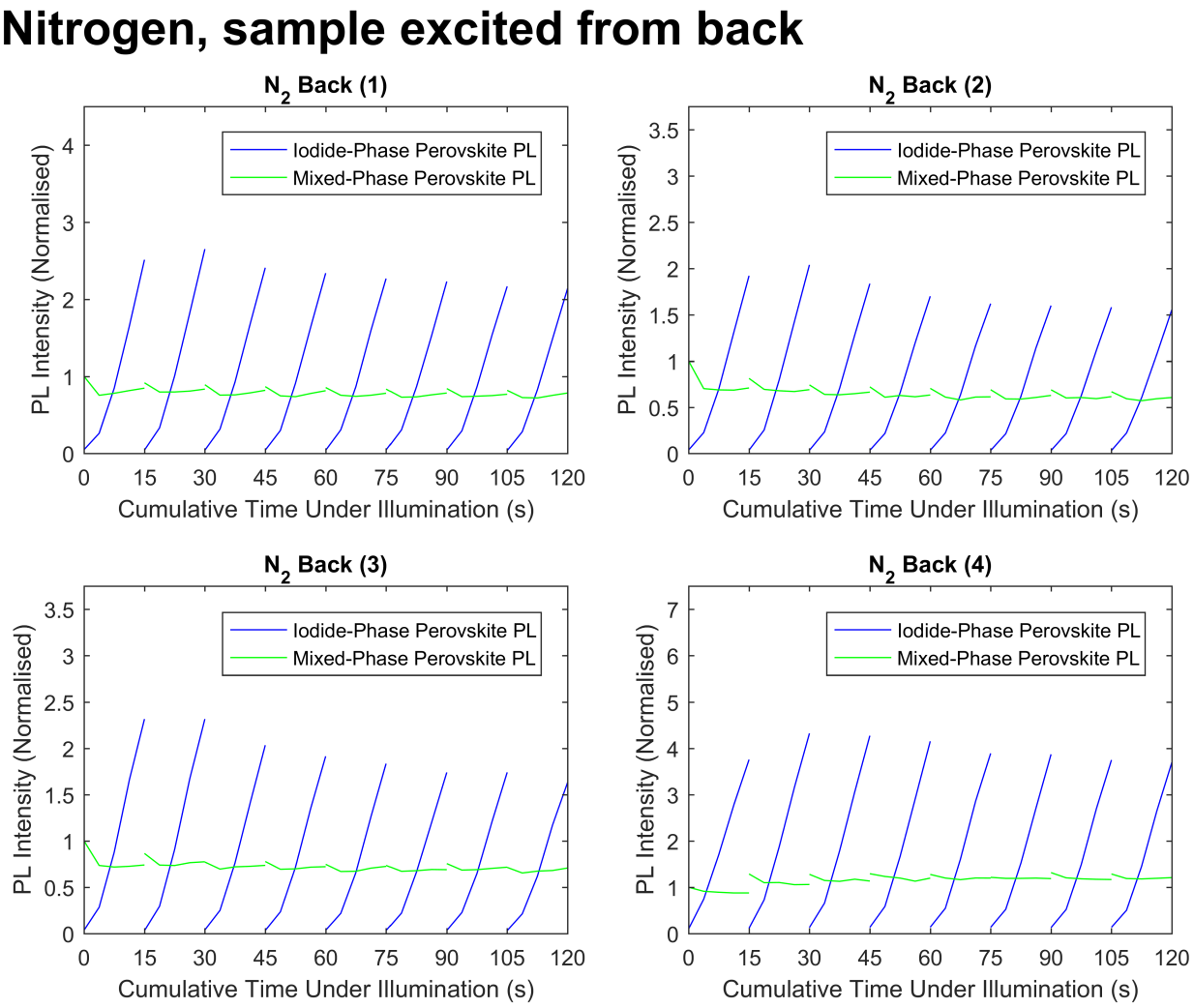

Figure S10: PL data highlighting the reversibility of halide segregation when $MAPb(Br_{0.5}I_{0.5})_3$ films are held under pressurized nitrogen (around 2 bar) and illuminated from the back (the substrate side). To induce repeated segregation and remixing, the films were exposed to 8 illumination cycles, with a single cycle consisting of 15 seconds of illumination followed by 30 minutes of darkness. Illumination was achieved with a 400 nm wavelength laser at AM1.5 equivalent power (see Section S3). The blue lines show the integrated intensity of the iodide-rich phase PL peak (around 720 nm to 770 nm) and the green lines the integrated intensity of the mixed-halide phase PL peak (around 640 nm to 690 nm), both normalized such that the initial mixed-phase measurement is set to 1.

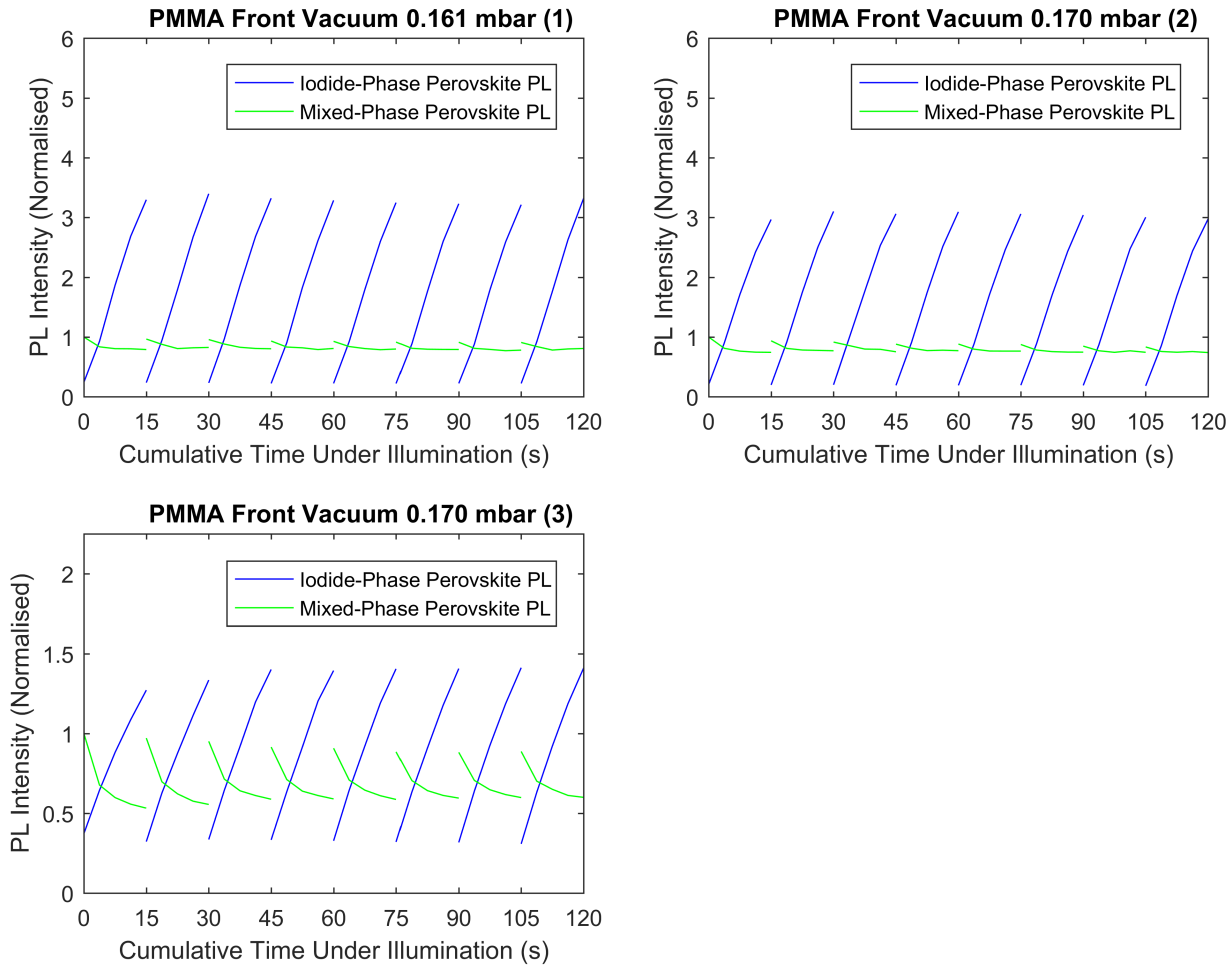

Figure S11: PL data highlighting the reversibility of halide segregation when PMMA coated $MAPb(Br_{0.5}I_{0.5})_3$ films are held under vacuum and illuminated from the front (the film side). To induce repeated segregation and remixing, the films were exposed to 8 illumination cycles, with a single cycle consisting of 15 seconds of illumination followed by 30 minutes of darkness. Illumination was achieved with a 400 nm wavelength laser at AM1.5 equivalent power (see Section S3). The blue lines show the integrated intensity of the iodide-rich phase PL peak (around 720 nm to 770 nm) and the green lines the integrated intensity of the mixed-halide phase PL peak (around 640 nm to 690 nm), both normalized such that the initial mixed-phase measurement is set to 1.

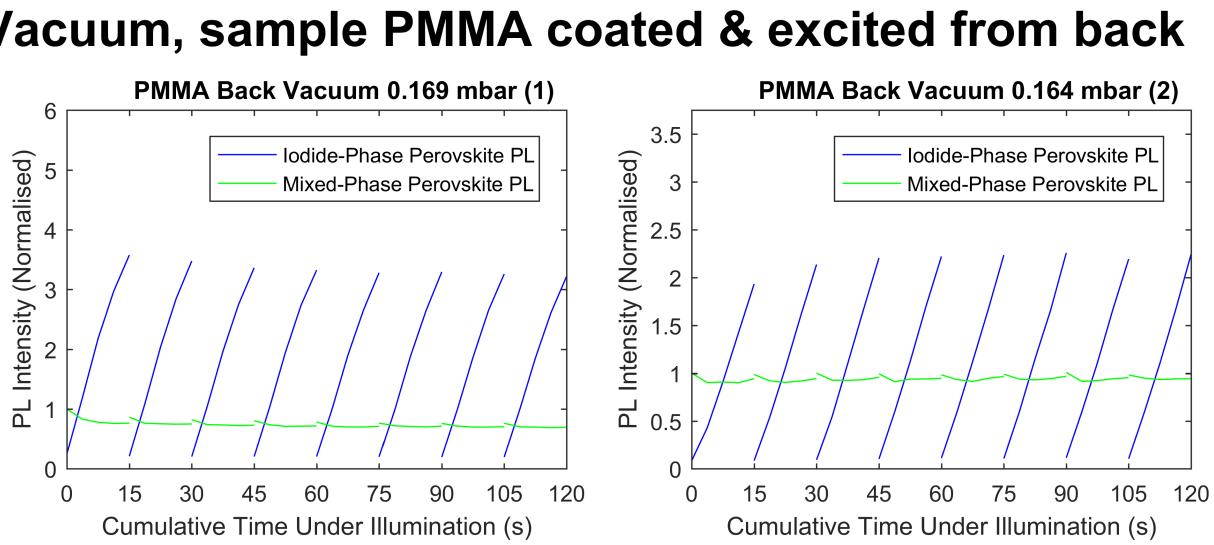

Figure S12: PL data highlighting the reversibility of halide segregation when PMMA coated $MAPb(Br_{0.5}I_{0.5})_3$ films are held under vacuum and illuminated from the back (the substrate side). To induce repeated segregation and remixing, the films were exposed to 8 illumination cycles, with a single cycle consisting of 15 seconds of illumination followed by 30 minutes of darkness. Illumination was achieved with a 400 nm wavelength laser at AM1.5 equivalent power (see Section S3). The blue lines show the integrated intensity of the iodide-rich phase PL peak (around 720 nm to 770 nm) and the green lines the integrated intensity of the mixed-halide phase PL peak (around 640 nm to 690 nm), both normalized such that the initial mixed-phase measurement is set to 1.

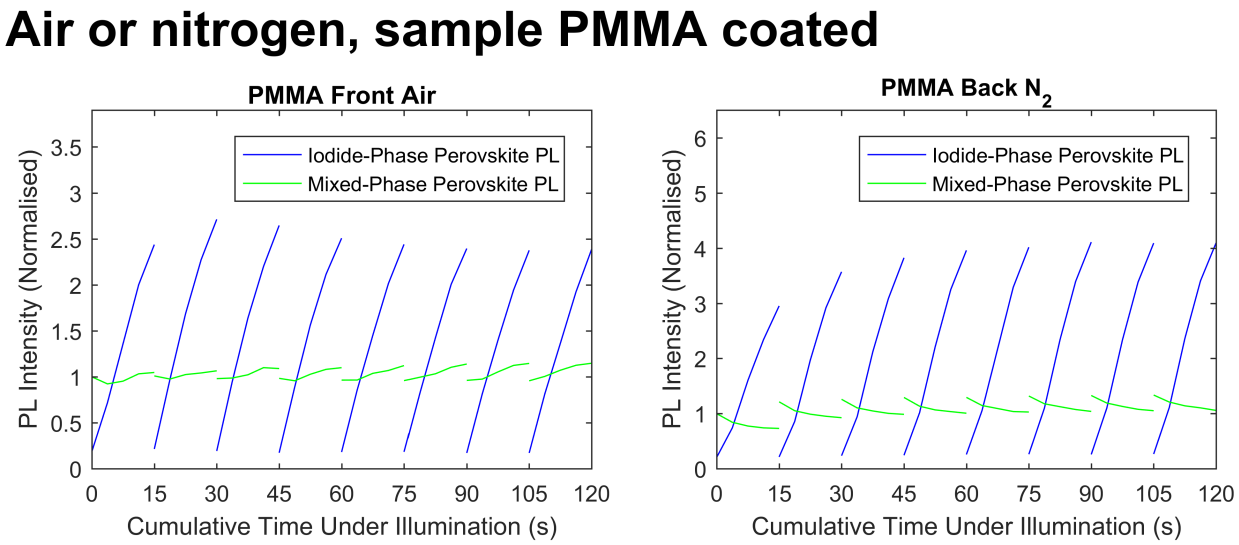

Figure S13: PL data highlighting the reversibility of halide segregation when PMMA coated $MAPb(Br_{0.5}I_{0.5})_3$ films are held under either air or pressurized nitrogen (2 bar). To induce repeated segregation and remixing, the films were exposed to 8 illumination cycles, with a single cycle consisting of 15 seconds of illumination followed by 30 minutes of darkness. Illumination was achieved with a 400 nm wavelength laser at AM1.5 equivalent power (see Section S3). The blue lines show the integrated intensity of the iodide-rich phase PL peak (around 720 nm to 770 nm) and the green lines the integrated intensity of the mixed-halide phase PL peak (around 640 nm to 690 nm), both normalized such that the initial mixed-phase measurement is set to 1.

5 Halide Segregation and Exposure Time

Figure 2a in the main text shows the results from an experiment concerning the change in halide segregation rate as the generation rate of photoexcited charge carriers was altered and the total number of incident photons per cubic centimeter was kept constant at $4.5 \times 10^{23}\,\mathrm{cm}^{-3}$. The sample used was a PMMA-coated $MAPb(Br_{0.5}I_{0.5})_3$ perovskite film held under vacuum which was always illuminated on the same spot. The sample was held in darkness for around 45 minutes between measurements to allow for a complete recovery from the induced halide segregation. In order to change the charge carrier generation rate at constant total incident photons per unit volume, the film was illuminated for different lengths of exposure time under correspondingly strong illumination intensities. The illumination source used was a 400 nm wavelength diode laser (Picoharp, LDH-D-C-405M) under continuous wave conditions. The PL from the sample was collected and coupled into a grating spectrometer (Princeton Instruments, SP-2558) which separated the light spatially by its wavelength. This light was measured by an iCCD camera (PI-MAX4, Princeton Instruments). A spectral integral over the range 640 nm to 690 nm was taken and defined as our measurement of the mixed-phase perovskite PL peak, and a similar spectral integral over the range 720 nm to 770 nm was used to define our measurement of the iodide-rich perovskite PL peak (see Figure S4 for the PL spectrum of our samples). It is noted that the limits of these spectral integrals have some minor effects on the analysis presented in this section. In order to provide a measure of halide segregation in terms of the relative peak amplitudes, independent of the different illumination powers used, the iodide-rich PL measurements were normalized such that the initial integrated intensity of the mixed-phase peak was set to 1. It is these normalized PL measurements that are plotted in Figure 2a and fitted with Equation S1 below.

The empirical equation used to fit the growth of the relative, integrated iodide-rich per-

ovskite PL peak, $I_{(\text{I-rich PL})}$, over the different exposure times is as follows:

$$I_{(\text{I-rich PL})} = f(gGt) = A\frac{(gGt)^2}{(1+(gGt)^2)}(1-e^{-BgGt}) \quad (1)$$

Here G is the is the generation rate of excited charge carriers per unit volume measured in $\text{cm}^{-3}\,\text{s}^{-1}$, t is time, A is a dimensionless global fitting parameter that is dependent on the exact method used to define $I_{(\text{I-rich PL})}$ and measured to be 43.6 for our definition explained above, B is a dimensionless global parameter determined from fits to be 27.5×10^{-3} , and g is the local fitting parameter that represents the scaling of the x-axis, given in centimetres cubed. g represents the degree of segregation caused in a unit volume of perovskite per excited charge carrier, and so can be described as a charge carrier efficacy. We note that a purely exponential form has been previously used to empirically fit the rise in iodide-rich phase PL signal as the perovskite segregates,[S5] however we find that our somewhat modified function is necessary to capture the initial slow rise of signal displayed in Figure S15. A and B were globally fitted to all eight exposure time curves simultaneously and are constants which define the general shape of Equation S1 without depending on exposure time. g, however, was fitted to each curve individually and so consequently is a function that has a different value for each exposure time. Because $I_{(\text{I-rich PL})}$ is a function of $g \times G \times t$ only, g represents a scaling parameter that scales the time axis of the low-bandgap PL growth depending on the exposure time measured under. For example, at $g = 1$, twice as much time – at constant G – is required to increase the low-bandgap PL intensity by the same amount as at $g = 2$, however the shape of the PL growth curve is similar across both cases. As a result of the nature of g, an overlay of every low-bandgap PL curve is achieved by multiplying the x-axis of each individual curve at different exposure times by the corresponding value of g, and this overlay is shown in Figure S14. Thus, instead of every data set being plotted from 0 to 4.5×10^{23} photons per centimeter cubed as in Figure 2a of the main text, each data set is individually plotted against $g \times G \times t$, where the value of g depends on the exposure time

of that data set. As an example, the value of g for the shortest exposure time, 6 seconds, is $5.95 \times 10^{-24}\,\mathrm{cm}^3$, so the PL data set taken over the 6 second exposure time would be plotted from $g \times G \times t = 0$ to 2.68 dimensionless units. The longest exposure time, 1044 seconds, corresponds to a value of g of $129 \times 10^{-24}\,\mathrm{cm}^3$, and so this data set is plotted from $g \times G \times t = 0$ to 58.2 dimensionless units. Table S1 lists the value of g for each exposure time and Figure S16 plots g versus exposure time. The dimensionless quantity, $g \times G \times t$, is the charge carrier efficacy (the degree of segregation of a unit volume caused per excited charge carrier) multiplied by the rate of incident photons per unit volume, multiplied by time, and so is a measure of the amount of segregation experienced by the film. It is an arbitrary measure of halide segregation, as it is defined by the choice of fitting function in Equation S1.

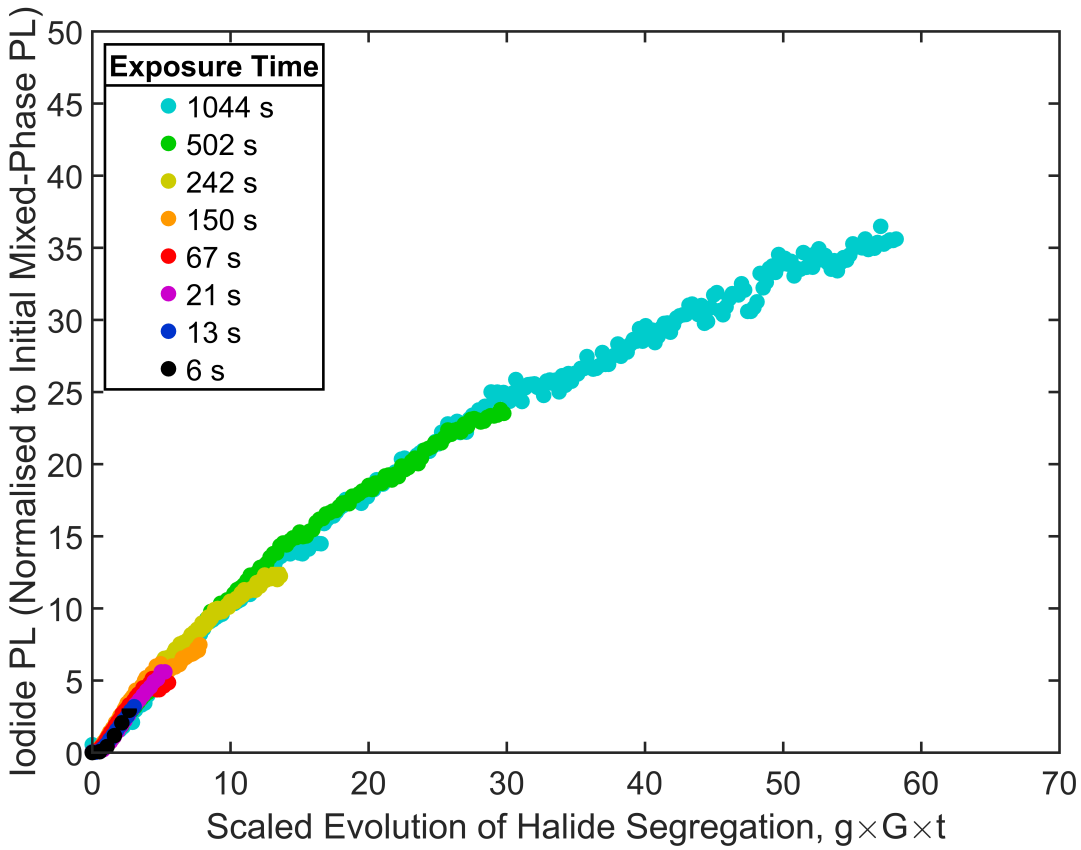

Figure S14: The evolution of the integrated iodide-rich perovskite PL signal under different illumination exposure times as a function of the scaling factor, g, times the cumulative number of incident photon number per unit volume, $G \times t$. The scaled cumulative number of incident photon number per unit volume, $g \times G \times t$, is a dimensionless measure of halide segregation. The PL signal is normalized such that the initial mixed phase perovskite PL signal (not shown) is set to 1 for each exposure time. The good overlay suggests that the underlying segregation mechanism remains the same across the charge carrier generation rates explored here.

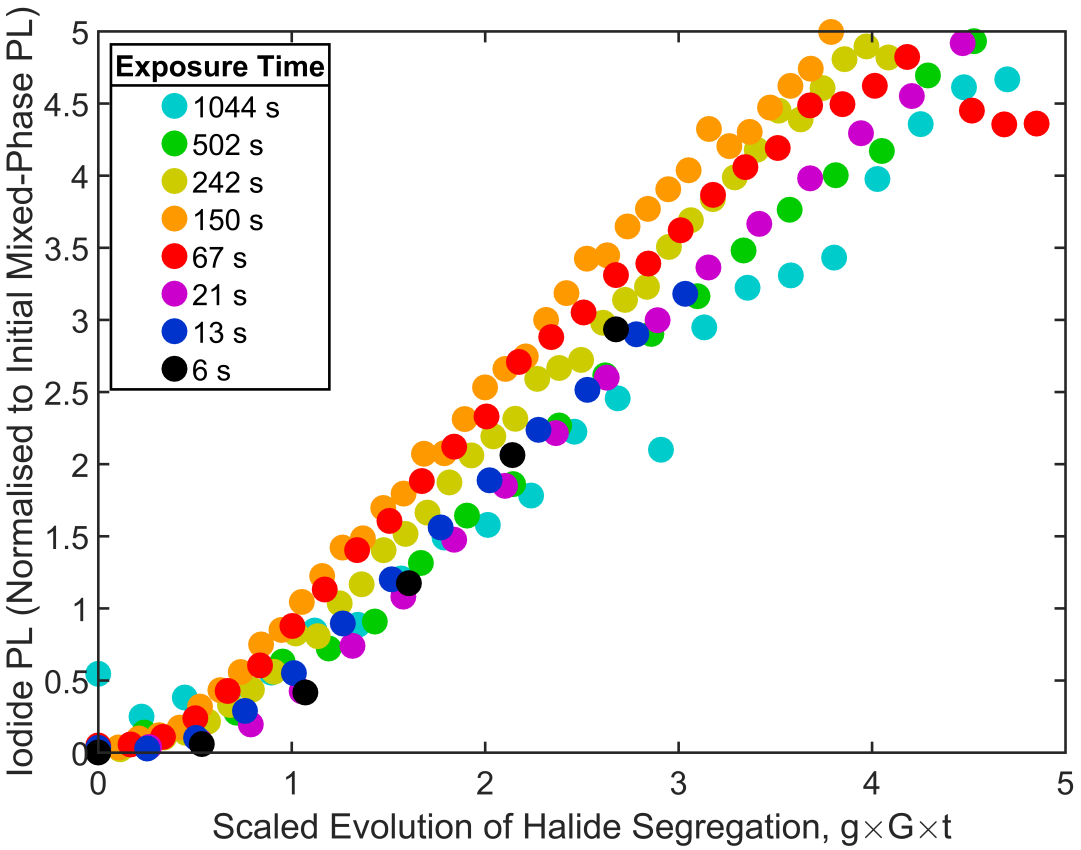

Figure S15: Zoomed section of Figure S14 to show the non-linear rise of low-bandgap PL at small values of $g \times G \times t$.

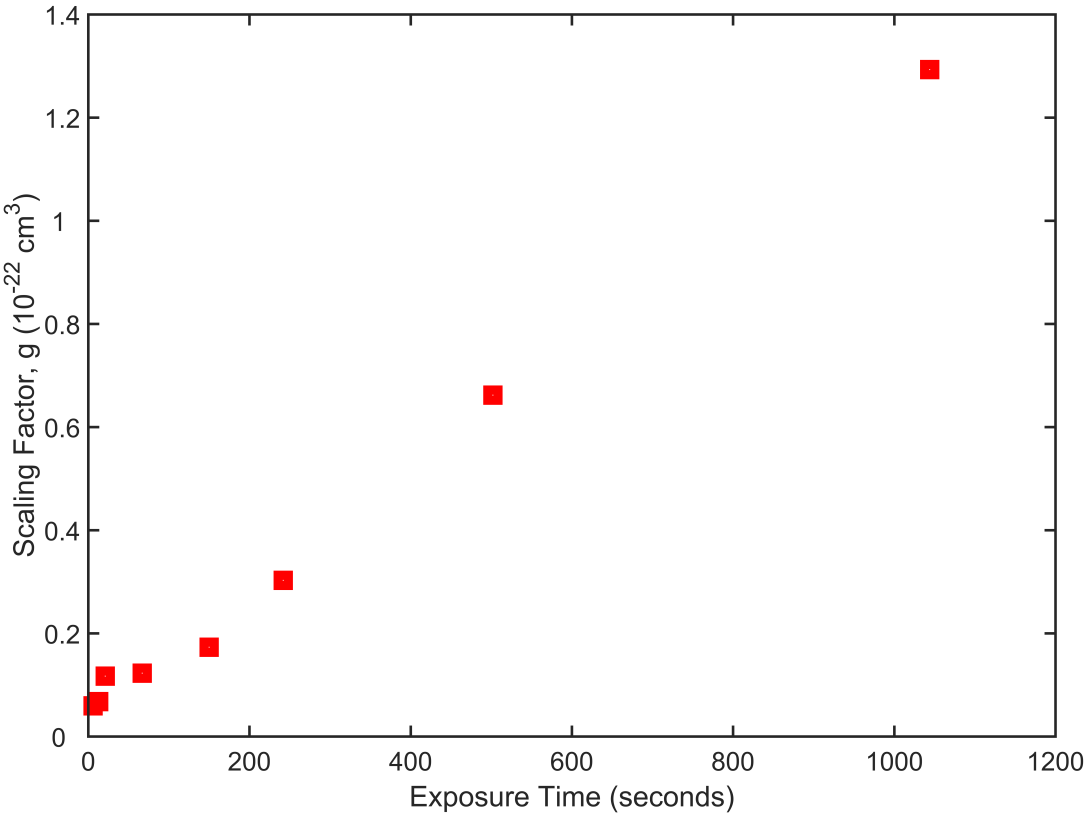

Figure S16: The values of the scaling factor, g, extracted from fits of Equation S1 to the data shown in Figure 2a of the main text, plotted against the corresponding exposure times of that same data. The seemingly linear trend of the last three data points is attributed to the longer exposure times used in these experimental runs allowing for a greater movement of the halide ions, and thus higher values of g, despite the saturation of the fraction of trap-mediated recombination.

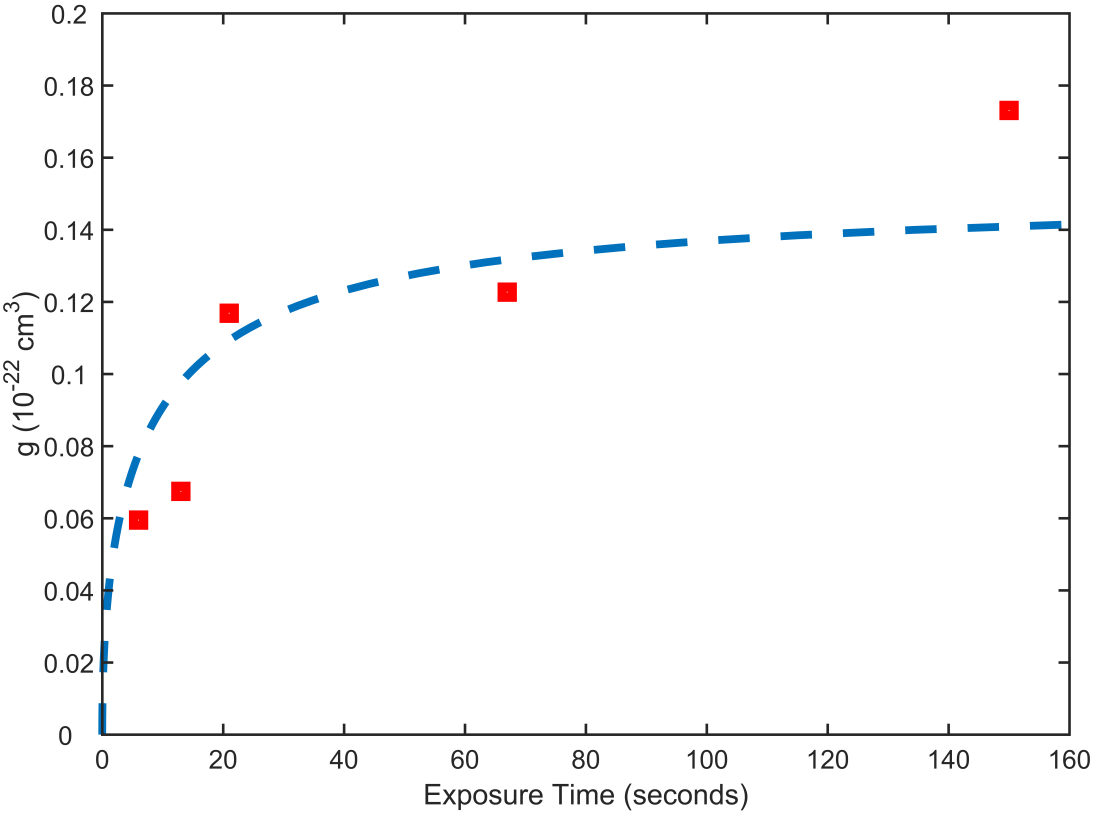

Figure S17: Zoomed section of Figure S16 showing the non-linear region of the data where the fraction of trap-mediated decay is the dominant factor in the halide segregation dynamics. The dashed blue line shows the fit used in Figure 2b of the main text: a linear fit when plotted against fraction of trap-mediated decay, however shown here to be non-linear when plotted against sample exposure time to illumination at constant total incident photons.

6 Fraction of Charge Carriers that Recombine Through Trap States

In the main text we propose that charge carriers recombining through trap states are responsible for halide segregation. In general, the charge carrier dynamics in a semiconductor are governed by five processes: stimulated absorption, stimulated emission, spontaneous emission, Shockley-Read-Hall recombination and Auger recombination.[S6] The first process, stimulated absorption,[S6,S7] occurs when a the material absorbs a photon by promoting a valence band electron to the conduction band. As a result of energy conservation, the incoming photon must have an energy higher than that of the bandgap to ensure the promoted electron can reach an unfilled energy state. Stimulated absorption is responsible for the generation of free charge carriers in a perovskite material under illumination, whereas the remaining charge carrier processes are concerned with the demotion of free electrons back to the valence band. Stimulated and spontaneous emission,[S6,S7] two such demotion processes, release the excess energy of the recombining charge carriers through the release of a photon. Stimulated emission requires an above-gap photon to initiate the demotion and light-emission process, whereas spontaneous emission occurs spontaneously. These two processes encapsulate the possible ways in which an excited electron may recombine with a hole while emitting an above-bandgap photon, *i.e.* they represent the possible radiative recombination processes. Stimulated absorption, stimulated emission and spontaneous emission are all intrinsic to a semiconducting material as they depend on the band structure and the nature of the incident illumination, and as such they are permanent mechanisms within any semiconductor under light. It can be shown that under strong illumination, the rate of radiative recombination processes in an intrinsic semiconductor scales with n^2, the charge carrier density squared.[S6] As a very basic argument, the probability of an excited electron transitioning to a valence band energy state will be proportional to the density of excited electrons available for the transition, times the density of available energy states to transition into. The proportionally

constant in this case corresponds to the quantum mechanical transition probability, among other factors. Due to the fact the perovskite samples under investigation in this work are – as a first approximation – intrinsic semiconductors, the density of available valence band states is equal to the number of excited, conduction band electrons, hence the overall n^2 dependence of the transition rate.

Shockley-Read-Hall (SRH) recombination, or trap mediated recombination, is a recombination process involving a localized trap state.[S6,S8,S9] Depending on the nature of the trap state situated in the bandgap, either an electron is caught and localized on the trap, before recombining with a free hole, or a hole is caught before recombining with a free electron. The excess energy of the charge carriers is typically carried away in lattice vibrations (phonons) making this process non-radiative, although it is possible for below-gap photons to carry away the additional energy. Because this process is intimately linked with the nature, energy, and density of the trap states within the semiconducting material, it is possible to alter the rate of SRH recombination through control of the material quality.[S6,S8,S9] Under the assumptions of an intrinsic semiconductor under intense illumination, it can be shown that the rate of SRH recombination is proportional to n.[S6,S8,S9] As an extremely simple argument, the rate of capture of either charge carrier type by a trap state should be proportional to the density of the relative charge carrier – both equal to n – times the density of available trap states. The de-trapping process, from similar logic, is then proportional to the density of filled traps times the density of opposing charge carriers – also equal to n. Assuming a high enough trap state density means that both these steps in the SRH process are controlled by n, and thus overall the recombination process scales with n.

Finally, Auger recombination processes constitute interactions between three charge carriers that result in the annihilation of an electron and a hole, with the excess energy and momentum absorbed by the third free charge carrier and potentially used in the emission of phonons.[S6] The excitation of the third charge carrier results in either an electron high in the conduction band, or a hole low in the valence band. As a result of the high number of

free charge carriers required, Auger processes generally become dominant at high illumination intensities, or when other recombination processes are limited such as in an extremely pure semiconductor with an indirect bandgap.[S6] As no photons are emitted, Auger processes contribute to non-radiative recombination in semiconductors, and due to the band-to-band nature of the process, Auger recombination is intrinsic to the semiconducting material and not directly dependent on the quality of the material. As a similar argument to the one for radiative and SRH recombination above, Auger recombination concerns the interaction of three free charge carriers and so scales with n^3.[S6]

Combining all three dependencies for the processes above, the following rate equation is arrived at:

$$\frac{\mathrm{d}n}{\mathrm{d}t} = G(t) - k_1 n - k_2 n^2 - k_3 n^3 \tag{2}$$

Here n is the charge carrier density, t is time, $G(t)$ is the generation rate of photoexcited charge carriers, and k_1, k_2 and k_3 are the first-, second- and third-order recombination rate constants respectively. $k_1 n$ represents SRH recombination and so is highly dependent on film properties such as the density of trap states, whereas $k_2 n^2$ and $k_3 n^3$ represent radiative and Auger recombination respectively and hence depend mostly on intrinsic material properties such as the band structure. $G(t)$ represents the rate of stimulated absorption, which is dependent on the illumination source, and so it is modeled differently depending on the exact nature of the experiment. Here we will discuss two common illumination methods: pulsed illumination where the sample is irradiated with short, repeated, concentrated pulses of light; and continuous wave illumination where the rate of incident photons on the sample is constant. The pulsed illumination calculation applies to the work of Yang *et al.*,[S10] which we use in the main text and in Section S7 to highlight the importance of the fraction of charge carriers that decay through trap states on halide segregation, whereas the continuous wave calculation applies to our own PL experiments, both those discussed here and in the main text.

Under pulsed laser illumination, charge carriers are photoexcited in a short amount of

time by a light pulse and recombine in the period of darkness before the subsequent light pulse arrives. Assuming all the generation from a pulse happens instantaneously – valid for a small pulse width – the time period of stimulated absorption is negligible, and we set $G(t) = 0$ in Equation S2 in order to describe the charge carrier dynamics in the respite period before the next pulse:

$$\frac{\mathrm{d}n}{\mathrm{d}t} = -k_1 n - k_2 n^2 - k_3 n^3 \tag{3}$$

Here, as before, n is the charge carrier density, t is time, and k_1, k_2 and k_3 are the first-, second- and third-order recombination constants respectively. The initial density of charge carriers, n_0, is calculated from the number of photons in the incident light pulses, which assumes that there are no excited charge carriers remaining from the previous light pulse. This assumption is generally very good, unless an extremely high pulse fluence or repetition rate is used, in which case charge carriers may survive across multiple measurements, a process that causes "wrap-around". $n(t)$ can then be solved for numerically, and the rate of change of the charge carrier density through monomolecular decay processes is then $k_1 n(t)$. This change in charge carrier density from monomolecular decay processes is then integrated over the time between light pulses to produce the number of charge carriers that decay through trap mediated channels per unit volume per pulse, $\int k_1 n(t)\mathrm{d}t$. This quantity then divided by the photoexcited charge carriers per unit volume per pulse, n_0, produces the fraction of charge carriers that recombine through trap states averaged over one pulse, $\frac{\int k_1 n(t)\mathrm{d}t}{n_0}$.

Under continuous wave illumination, charge carriers are constantly photoexcited and constantly recombine, with the stimulated emission process incorporated into Equation S2 as a constant generation rate, $G(t) = G$. The generation rate is calculated from: $G = \frac{P}{VE}$, where P is the laser power, V is the volume of photoexcited perovskite, and E is the photon energy of the illumination. This constant form of G assumes a uniform charge carrier density throughout the film, which should be valid given that the photogenerated charge carriers

quickly spread out due to diffusion and photon recycling to give an even profile.[S4] The inclusion of G, alongside setting $\frac{\mathrm{d}n}{\mathrm{d}t} = 0$ to calculate for the steady-state dynamics, results in the following equation:

$$k_3 n^3 + k_2 n^2 + k_1 n - G = 0 \tag{4}$$

From Equation S4 the fraction of all generated charge carriers that recombine non-radiatively, $\frac{k_1 n}{G}$, can be calculated.

In order to apply the continuous wave analysis above to our PL experiments, values of $k_1 = 5 \times 10^6\,\mathrm{s}^{-1}$ and $k_2 = 6 \times 10^{-10}\,\mathrm{cm}^3\,\mathrm{s}^{-1}$ were measured for our perovskite films through time correlated single photon counting techniques, detailed in section S8. k_3 is assumed to be similar to other lead-based perovskites[S11,S12] at around $1 \times 10^{-28}\,\mathrm{cm}^6\,\mathrm{s}^{-1}$. In order to calculate the generation rate, G, the thickness of our films was determined from cross-sectional SEM images to be 390 nm (see Section S2), the illumination spot size was measured to be $0.0148\,\mathrm{mm}^2$, and the emission wavelength of the illumination laser used was noted to be 400 nm. Table S1 then shows the results of incorporating these parameters into Equation S4 for the laser powers used at each exposure time. Additionally shown is the scaling factor g (extracted from fits of Equation S1) for each exposure time.

Table S1: The fraction of charge carriers that recombine through trap states and scaling factors for the different exposure times used by us to collect the data shown in Figure 2a of the main text.

Exposure Time (seconds)	Charge Carrier Generation Rate ($\mathrm{cm}^{-3}\,\mathrm{s}^{-1}$)	Fraction of Charge Carriers that Recombine Through Trap States, $\frac{k_1 n}{G}$	Scaling Factor and Charge Carrier Efficacy, g (cm^3)
6	7.5×10^{22}	0.51	5.95×10^{-24}
13	3.5×10^{22}	0.64	6.74×10^{-24}
21	2.1×10^{22}	0.73	11.7×10^{-24}
67	6.7×10^{21}	0.88	12.3×10^{-24}
150	3.0×10^{21}	0.94	17.3×10^{-24}
242	1.9×10^{21}	0.96	30.3×10^{-24}
502	9.0×10^{20}	0.98	66.2×10^{-24}
1044	4.3×10^{20}	0.99	129×10^{-24}

7 Dependence of Halide Segregation on Pulse Frequency

Yang *et al.* observed a relation between the apparent rate of halide segregation in $MAPb(Br_{0.57}I_{0.43})_3$ films and the laser repetition rate of the pulsed illumination used to illuminate the samples at a constant average intensity.[S10] In order to achieve a constant average illumination intensity when changing the laser repetition rate, Yang *et al.* altered the instantaneous pulse intensity correspondingly. Here we show that the repetition rate of pulsed illumination does not influence the rate of halide segregation in similar $MAPb(Br_{0.5}I_{0.5})_3$ films when the pulse width, rather than the pulse intensity, is altered to keep the average intensity constant. Figure S18 shows schematics of the changes in illumination profile when Yang *et al.* increased the illumination repetition rate at constant pulse width (Figures S18(a) to (b)), and when we increased the illumination repetition rate at constant instantaneous intensity (Figures S18(c) to (d)), while we both ensured the average illumination power remained constant. Our results strongly suggest that halide segregation depends on the instantaneous intensity of pulse illumination, and rules out the possibility that the repetition frequency of illuminating light pulses directly affects halide segregation.

In order to change the separation and the pulse width of the illuminating light pulses, a mechanical chopper was inserted into our beam line before the sample chamber. A chopper is a component consisting of a rapidly rotating disk with holes that alternatively block and pass the beam, creating a square-wave modulation of the light. The nature of this component means that the instantaneous illumination power of the pulses is constant regardless of the frequency of the chopper, see Figures S18(c) and (d) for schematics of the time-dependent illumination through a chopper. The constant instantaneous intensity of a laser pulse resulting from the chopping procedure, alongside the fact that the charge carrier lifetimes ($\sim 0.1\,\mu s$) are negligible compared to the pulse widths measured over ($> 200\,\mu s$), means that the fraction of charge carriers that recombine through trap states in our films does not change with chopper frequency.

In order to test the dependence of halide segregation rate on the repetition frequency of

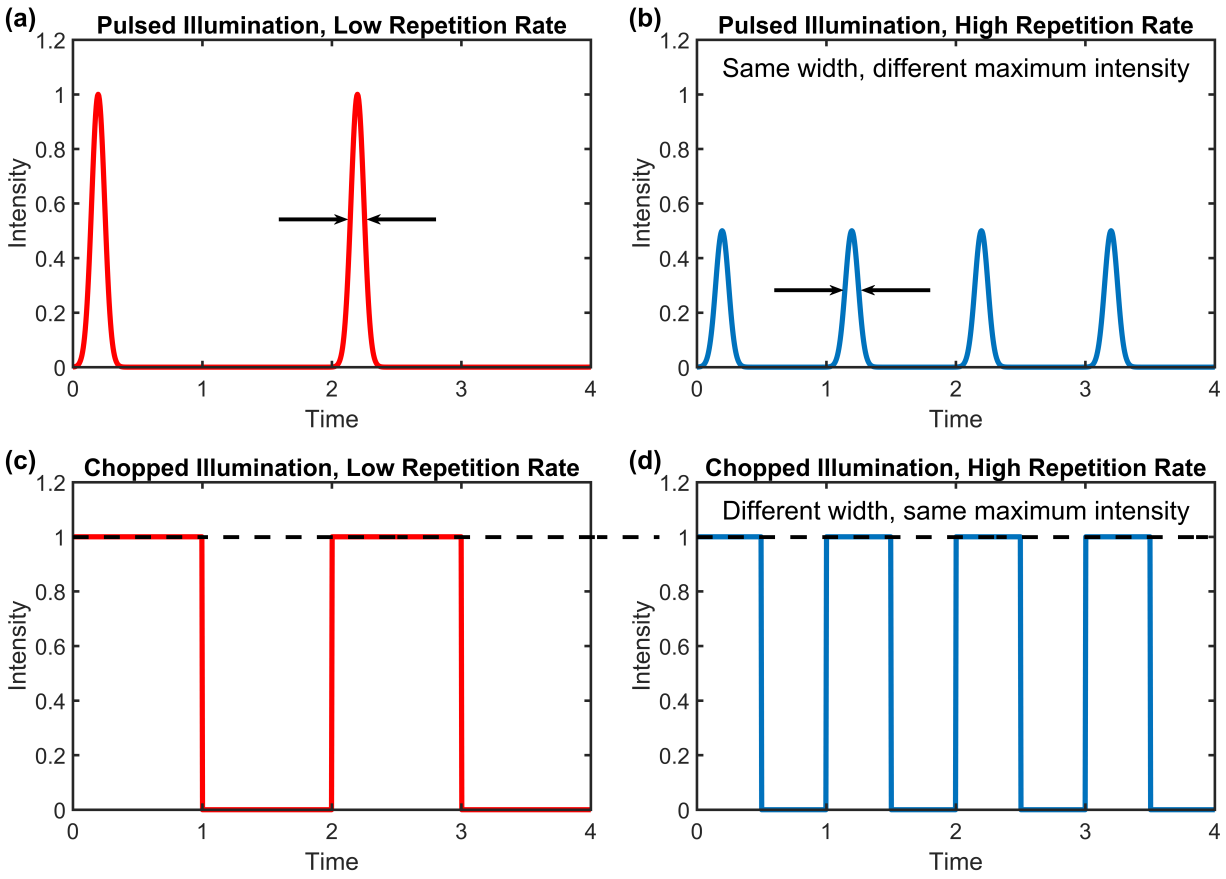

Figure S18: Schematic showing two different methods in which to change the repetition rate of incident illumination without changing the average intensity. (a) and (b) show that under pulsed illumination, as in the work of Yang *et al.*, the width of the light pulses remains constant, so the maximum intensity must be reduced to keep the average intensity constant. Lowering the maximum intensity then lowers the density of charge carriers excited by each pulse. (c) and (d) show that under chopped, continuous wave illumination, as in our work, the pulse width changes with repetition rate, however the illumination intensity remains constant. A constant illumination intensity results in a constant density of photoexcited charge carriers, regardless of the illumination repetition rate.

chopped laser pulses, a PMMA coated $MAPb(Br_{0.5}I_{0.5})_3$ perovskite film held under vacuum was used as a sample, and the same spot of the sample was illuminated over the course of the experiment. The illumination was provided by a 400 nm wavelength diode laser (Picoharp, LDH-D-C-405M) under continuous wave conditions at AM1.5 equivalent average power (see Section S3). The sample was left in at least 30 minutes of darkness between measurements. The chopper was a Standford Research Systems optical chopper, model SR540, utilized with either the 6 slot or 30 slot chopper blade setup depending on the repetition rate required.

The PL from the sample was collected and coupled into a grating spectrometer (Princeton Instruments, SP-2558) which separated the light spatially by its wavelength. This light was measured by an iCCD camera (PI-MAX4, Princeton Instruments).

We observed no difference to the evolution of the iodide-rich phase PL signal as the frequency was changed over two and a half orders of magnitude, see Figure S19. The results from our experiment show that the repetition rate of the incident illumination does not directly affect the rate of halide segregation, suggesting that the changes in segregation rate observed by Yang *et al.* were caused by the change in pulse fluence required to keep the average illumination power constant when the repetition rate was changed. In the main text, we established that the fraction of charges that recombine through trap states is linked with the rate of halide segregation. We shall now demonstrate that the changes in pulse fluence in the work of Yang *et al.*[S10] altered the monomolecular decay fraction as the repetition rate of the incident illumination was changed. Our empirical model for halide segregation qualitatively matches the results observed by Yang *et al.* to a high degree of accuracy.

Yang *et al.* used a pulsed laser to illuminated their samples, and so from the analysis done in Section S6, Equation S3 describes the charge carrier dynamics in the films between laser pulses. In order for our empirical model to predict the levels of halide segregation experienced by the films, the average fraction of charge carriers that recombine through trap states, $\frac{\int k_1 n \mathrm{d}t}{n_0}$, must be calculated though numerically solving Equation S3 for $n(t)$ and evaluating the initial charge carrier density excited by each laser pulse, n_0. In order for the pulse-averaged, rather than the time-dependent, monomolecular decay fraction to be accurate for our model, the timescales of the electronic decay processes (hundreds of nanoseconds) must be much faster than the migration time of the halide ions (tens of seconds), which is indeed the case here. Yang *et al.* report using a laser intensity of $50\,\mathrm{W\,m^{-2}}$ at a photon wavelength of 532 nm on 300 nm thick samples,[S10] which, assuming every incident photon generates a charge carrier, allows for the calculation of n_0 at each repetition rate (see Table S2 for

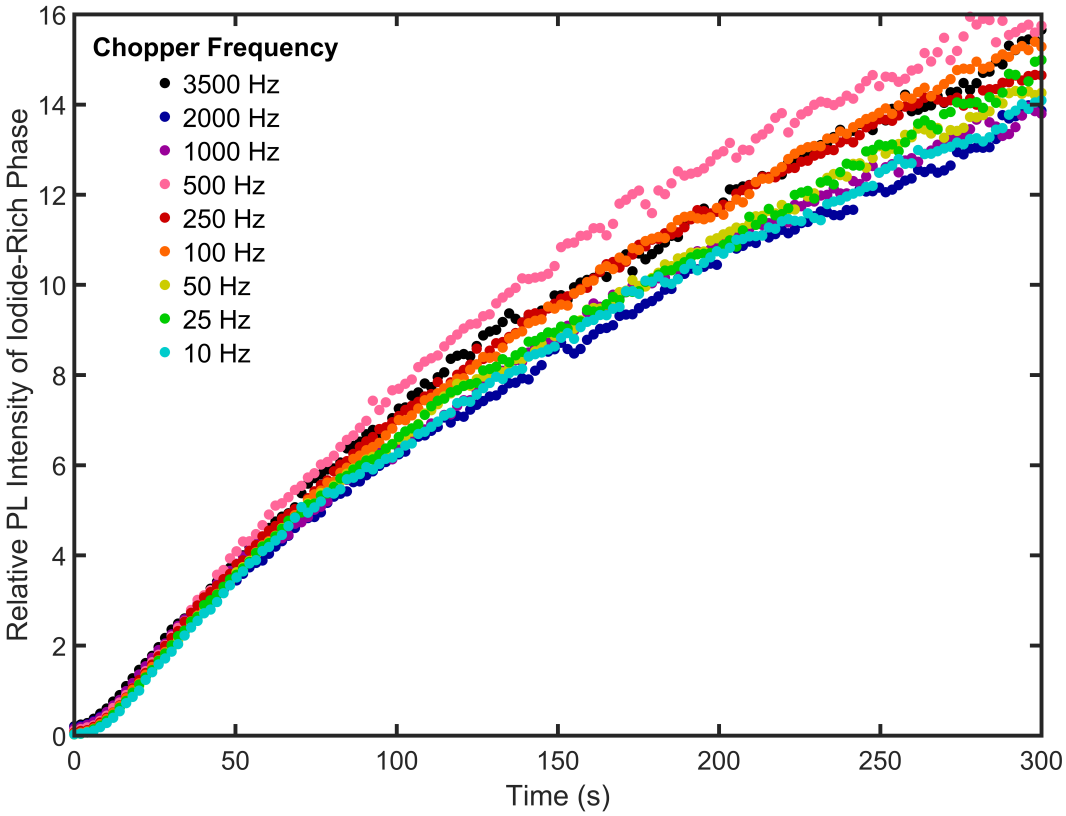

Figure S19: The increase in low-bandgap PL (integrated from around 720 nm to 770 nm) when normalized to the initial measurement of the mixed-phase PL peak (integrated from 640 nm to 690 nm) which is attributed to the formation of regions of iodide-rich perovskite from halide segregation under illumination through a chopper at various frequencies. The similar signal growth at all chopper frequencies displayed here shows that illumination pulse frequency has no direct effect on the halide segregation mechanics.

calculation results):

$$n_0 = \frac{\text{Laser Intensity}}{\text{Repetition Rate} \times \text{Photon Energy} \times \text{Film Thickness}} \tag{5}$$

The calculations of n_0 assume a spatially constant charge carrier density, a valid assumption given that the charge carriers spread out from diffusion and photon recycling processes on short time scales.[S4] k_1 is estimated from the PL transients reported by Yang *et al.*[S10] to be $50 \times 10^6\,\mathrm{s}^{-1}$, and k_2 and k_3 are taken to be similar to our and other perovskite compositions[S11] at $6 \times 10^{-10}\,\mathrm{cm}^3\,\mathrm{s}^{-1}$ and $1 \times 10^{-28}\,\mathrm{cm}^6\,\mathrm{s}^{-1}$ respectively, see Section S8. Inserting

these rate constants into Equation S3 and numerically solving allows for the calculation of $\frac{\int k_1 n dt}{n_0}$ at each repetition rate, see Table S2.

In order for our empirical model, described by Equation S1 and explained in the main text, to predict the induced level of halide segregation in a perovskite film, three input parameters are required: t, g and G. t is the time over which the segregation occurred, equal to 600 s in the experiments performed by Yang *et al.*[S10] g is the charge carrier efficacy, or scaling factor, that measures how effective a given photon is at inducing halide segregation. The empirical dependence between g and the monomolecular decay fraction is shown in Figure 2b of the main text, and using the fit to the linear regime of that figure (the first five data points), an estimated value of g can be extracted for a given fraction of charge carriers that recombine through trap states. This monomolecular decay fraction has been, through the methods discussed above, calculated for every laser repetition rate utilized by Yang *et al.*,[S10] with the results of these calculations shown in Table S2. Finally, G is the generation rate of charge carriers per unit volume, and so can be calculated from dividing the incident laser intensity by the photon energy and film thickness (which again assumes a uniform charge carrier density is valid[S4]). For Yang *et al.* this corresponds to:

$$G = \frac{50\,\mathrm{W\,m^{-2}}}{(3.7 \times 10^{-19}\,\mathrm{J}) \times (3 \times 10^{-7}\,\mathrm{m})} = 4.5 \times 10^{26}\,\mathrm{m^{-3}\,s^{-1}} = 4.5 \times 10^{20}\,\mathrm{cm^{-3}\,s^{-1}} \qquad (6)$$

Inserting t, g and G into Equation S1 generates the expected ratio of final, low-bandgap PL intensity to the initial, mixed-phase PL intensity, which is additionally shown in Table S2 for each laser repetition rate.

A direct comparison between our prediction of how much segregation should have been observed versus the amount of segregation actually observed by Yang *et al.*[S10] is shown in Figure 3 of the main text. The square data points in Figure 3 represent the experiments performed by Yang *et al.*, with the position of the squares calculated from the work carried out in this section, and the interior color of the squares indicating the *actual* amount of

iodide-rich phase PL observed by Yang *et al.*. Thus, if our empirical model is capable of predicting the level of induced halide segregation, the interior color of the squares (corresponding to Yang *et al.*'s observations) should match the color of their position in the color map (corresponding to our model). We find our predictions to be in excellent agreement with the actual observations, with the data point at 2 kHz predicted and observed to fall where the iodide-rich perovskite emission begins to dominate the PL spectrum.

Table S2: Various calculated parameters for the different laser repetition rates utilized by Yang *et al.* in their induction of halide segregation in $MAPb(Br_{0.57}I_{0.43})_3$.[S10] n_0 is calculated from the laser power, repetition rate, film thickness and photon energy reported by Yang *et al.*. The fraction of charge carriers that recombine through trap states is calculated through numerically solving Equation S3 for $n(t)$. The predicted ratio of final low-bandgap PL to initial PL is generated by Equation S1, and represents the degree of halide segregation the film undergoes under the corresponding laser repetition rate.

Laser Repetition Rate (Hz), Taken from[S10]	n_0 (cm^{-3}), Calculated from[S10]	Fraction of Charge Carriers that Recombine Through Trap States, $\frac{\int k_1 n dt}{n_0}$	Predicted Ratio of Final Low-Bandgap PL to Initial PL
100	4.46×10^{18}	0.066	~ 0.02
200	2.23×10^{18}	0.12	~ 0.1
500	8.92×10^{17}	0.22	~ 0.5
1,000	4.46×10^{17}	0.34	1.1
2,000	2.23×10^{17}	0.48	1.8
5,000	8.92×10^{16}	0.68	2.8
10,000	4.46×10^{16}	0.80	3.4
20,000	2.23×10^{16}	0.89	3.8
50,000	8.92×10^{15}	0.95	4.1
100,000	4.46×10^{15}	0.98	4.2
1,000,000	4.46×10^{14}	1.0	4.4

8 Time Correlated Single Photon Counting (TCSPC) Measurements

In order to extract the first- and second-order rate constants, k_1 and k_2 (see Section S6 for a discussion of charge carrier recombination processes) from our films, TCSPC measurements were performed on PMMA coated $MAPb(Br_{0.5}I_{0.5})_3$ films held under vacuum. The pulsed excitation was provided by a 400 nm wavelength diode laser (Picoharp, LDH-D-C-405M) at 5 MHz repetition rate. The PL from the samples was collected and coupled into a grating spectrometer (Princeton Instruments, SP-2558) fitted with a photon-counting detector (PDM series from MD) with the timing controlled by a PicoHarp 300 TCSPC Event Timer. In order to monitor changes that might occur as a results of the illumination, *e.g.* halide segregation, measurements were made over 320 seconds of illumination, which was separated into three accumulation time windows: 0-100 seconds, 110-210 seconds and 220-320 seconds. The PL was detected centered on two wavelengths of emitted photons at 660 nm and 740 nm to examine the mixed and iodide-rich perovskite phases in the perovskite, respectively. Furthermore, three illumination intensities were used to probe different charge carrier density regimes (1760, 500 and 110 $W\,m^{-2}$) and three repeats were performed and averaged over for each measurement. The measurements were all made on the same area of perovskite film, with at least 30 minutes left between measurements, and with 45 minutes or more left between measurements at the higher illumination powers. The data from these TCPSC measurements are shown in Figure S20.

The fitting of these data was complicated by the segregation of the films occurring as the measurements were taken. The formation of low-bandgap, iodide-rich regions of perovskite cause charge carriers to funnel out of the mixed phase and into these forming regions. This leads to three effects that could influence the results of a TCSPC measurement: 1) The movement of charge carriers between regions creates an extra "decay" mechanism for one region, and a new generation term for the other. 2) As the volume of the iodide-rich perovskite

changes, the density of charge carriers within those regions will change. 3) The movement of halide ions will change the microscopic properties of the film, which could in turn alter the values of k_1 though the evolution of trap states, and the measurements of k_2 through the re-absorption of photons and the channeling of charge carriers into iodide-rich regions where confinement effects may enhance k_2. In order to monitor these effects, the three accumulation windows were handled separately, so that any changes in the fitted values of k_1 and k_2 could be observed.

As discussed in Section S6, the rate of radiative recombination is approximately equal to $k_2 n(t)^2$ under certain film and illumination conditions, where n is the photoexcited charge carrier density, and t is time. TCSPC measurements record photons emitted from the photoexcited sample, making TCSPC sensitive only to radiative recombination and so to $k_2 n(t)^2$. Accordingly, in order to extract values for k_1 and k_2, a functional form for $k_2 n(t)^2$ is required to fit to the TCSPC data. Given that TCSPC measurements occur under pulsed laser conditions, the discussion in Section S6 explains that the charge carrier dynamics are governed by Equation S3. Rather than extract values for k_1 and k_2 simultaneously, we first devised a fitting method that would be sensitive to k_1 only. At low charge carrier density, such as at low excitation fluence or at times long after the pulse arrival, the dominant term in Equation S3 is $k_1 n$, and so the charge carrier dynamics are well approximated by:

$$\frac{\mathrm{d}n}{\mathrm{d}t} = -k_1 n \tag{7}$$

Solving Equation S7 for $n(t)$ results in the following equation for $k_2 n(t)^2$:

$$\text{PL Intensity} \propto k_2 n(t)^2 = k_2 n_0^2 e^{-2k_1 t} \tag{8}$$

Here n_0 is the charge carrier density initially generated by the laser pulse, and the other

symbols have been otherwise stated. Taking the natural logarithm of Equation S8 results in:

$$\ln\left(\frac{(k_2 n(t)^2)}{(k_2 n_0^2)}\right) = -2k_1 t \tag{9}$$

Thus, at low charge carrier densities, the gradient of the TCSPC data plotted on a log-lin scale is related only to the monomolecular decay rate constant, k_1.

The decay trails at the three different illuminations intensities become roughly parallel on a log-lin scale around 100 ns after the pulse arrival, see Figure S20, which indicates that after this time the charge carrier decay is being dominated by monomolecular pathways. We extract values for k_1 by fitting a single exponential function, ae^{-bt}, with fitting parameters a and b to this region and assuming the evolution of the measured counts is well described by Equation S8. k_1 was then taken as $\frac{b}{2}$ and the three values for k_1 extracted from the three different excitation fluences were then averaged over.

Table S3 presents the extracted values of k_1 from the two collection wavelengths and all three accumulations windows. The values are consistent with each other and similar films in the literature,[S11] and the average value of $5 \times 10^6\,\mathrm{s}^{-1}$ was taken as a representative value for all calculations in this SI and in the main text.

Table S3: Extracted values for k_1 from TCSPC measurements.

Wavelength (nm)	Accumulation Window (seconds)	Fitted k_1 (s^{-1})
660	0-100	5.04×10^6
660	110-210	5.57×10^6
660	220-320	5.43×10^6
740	0-100	4.60×10^6
740	110-210	4.84×10^6
740	220-320	4.55×10^6

In order to extract the value for k_2 from the TCSPC data (Figure S20), it is necessary to consider the regime in which the charge carrier density is high enough to induce a significant amount of radiative recombination (see Section S6 for a discussion of the recombination processes). It is assumed, however, that the charge carrier densities reached under the illumi-

nation intensities used ($< 1800\,\mathrm{W\,m^{-2}}$) does not significantly excite the higher-order Auger recombination processes. As a result of this assumption, the dynamics of the recombination processes are described by the following rate equation:

$$\frac{\mathrm{d}n}{\mathrm{d}t} = -k_1 n - k_2 n^2 \tag{10}$$

This equation can be solved analytically to find:

$$n(t) = \frac{k_1 n_0 e^{-k_1 t}}{k_1 + k_2 n_0 (1 - e^{-k_1 t})} \tag{11}$$

And so:

$$k_2 n(t)^2 = \frac{k_2 k_1^2 n_0^2 e^{-2k_1 t}}{(k_1 + k_2 n_0 (1 - e^{-k_1 t}))^2} \tag{12}$$

Equation S12, multiplied by a constant to take into account the imperfect outcoupling of photons emitted from radiative recombination to the measurement apparatus, was then fitted to the acquired TCSPC data (Figure S20) to extract values for k_2 and n_0. k_1 was fixed to $5 \times 10^6\,\mathrm{s^{-1}}$, the value extracted at low charge carrier density as previously discussed, and the value for n_0 was fitted to each graph individually because it was impossible to determine how it would develop as the charge carriers funneled into the forming regions of iodide-rich perovskite. k_2 was fitted globally across the three different excitation fluences, but not across the different measurement wavelengths or accumulation windows. The extracted values for k_2 are shown in Table S4, and the combined k_1, k_2 fitted functions are shown in Figure S20 alongside the TCSPC data.

Table S4: Extracted values for k_2 from TCSPC measurements.

Wavelength (nm)	Accumulation Window (seconds)	Fitted k_2 ($\mathrm{cm^3\,s^{-1}}$)
660	0-100	6.38×10^{-10}
660	110-210	6.22×10^{-10}
660	220-320	9.94×10^{-10}
740	0-100	9.28×10^{-10}
740	110-210	8.15×10^{-10}
740	220-320	8.36×10^{-10}

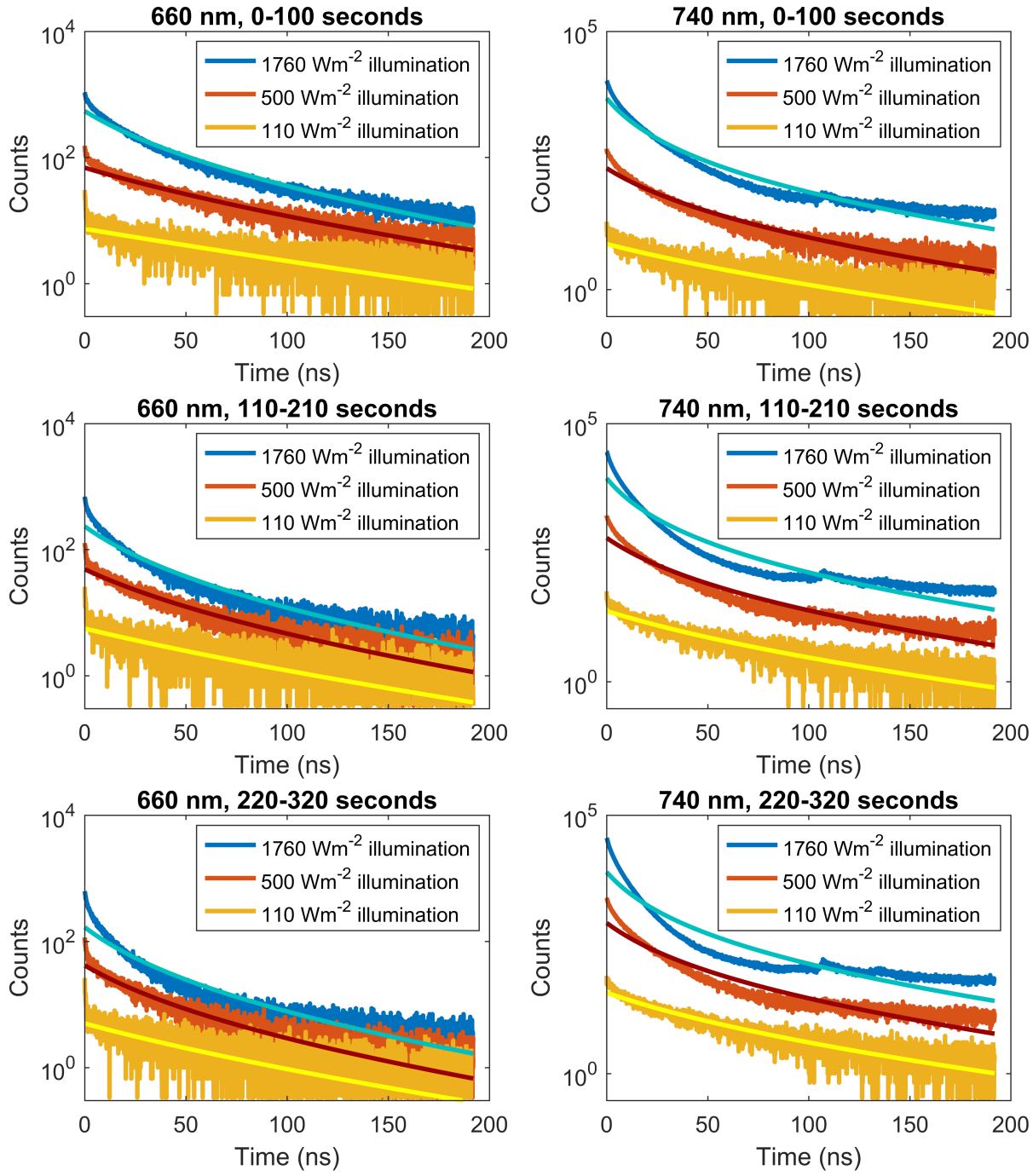

Figure S20: TCSPC data, taken at the mixed phase and iodide-rich perovskite PL peaks. Because the perovskite was segregating as the measurements were performed, three measurement windows of 0-100 s, 110-210 s and 220-320 s were used to observe how the decay curves changed over time. Three experimental repeats were performed for each condition and averaged over to produce these plots, and a trigger frequency of 5 MHz was used. The sample measured was a PMMA coated film under vacuum and the same spot was always illuminated within repeats. Between 30 and 45 minutes was left between each measurement.

The fits shown in Figure S20 highlight the tendency of the halide segregation mechanism to deviate the decay behavior away from the expected, "ideal" fitted functions. Correspondingly, the fitted functions appear most accurate at the earliest accumulation window, at the 660 nm measurement wavelength, and at the lowest excitation fluence, where the degree of halide segregation is lowest. Due to the variation in the extracted values of k_2, we did not average over them as we did for the value of k_1, but instead took the value of $6 \times 10^{-10}\,\mathrm{cm^3\,s^{-1}}$ extracted from the minimally segregated, 660 nm measurement wavelength, 0-100 s accumulation window decay trails. This value is in good agreement with other values reported in the literature for similar perovskite compositions.[S11]

9 AM1.5 Stability Calculation

From our data and analyses presented in this work, we are able to predict the trap-mediated charge carrier recombination rate for which a working $MAPb(Br_{0.5}I_{0.5})_3$ perovskite solar cell would not significantly undergo halide segregation over the course of one day under one sun illumination. To do so, the accumulative number of photons per unit volume incident upon the perovskite films under one sun must first be calculated. For the purposes of this calculation we shall assume perovskite films of similar thickness to ours: 390 nm. From Section S3 the rate of incident photons per unit volume upon such a film is $3.05 \times 10^{21}\,\mathrm{cm^{-3}\,s^{-1}}$, which is assumed to also be the generation rate of charge carriers within the perovskite film. We then define our point of "significant segregation" to be when the iodide-rich perovskite PL peak is of the same amplitude as the initial measurement of the mixed-phase PL peak, which corresponds to $I_{(\text{I-rich, PL})}=1$ in Equation S1. Inputting the relevant values for A, B, G and t into Equation S1 and setting $I_{(\text{I-rich, PL})}=1$ then allows us to find the value of g that will just prevent significant segregation under the given conditions. We therefore take A and B to be the values fitted from the analysis presented in Section S5, G to be $3.05 \times 10^{21}\,\mathrm{cm^{-3}\,s^{-1}}$ and t to be 12 hours, or 43200 seconds, and find the corresponding value of g to be $1.01 \times 10^{-26}\,\mathrm{cm^3}$.

This value of g is two orders of magnitude smaller than the range explored by our experiments, which reflects the extremely long exposure time of 12 hours used in this calculation. Thus at this point we highlight that the calculation presented in this section is speculative, however we believe there is some insight gained from continuing and extrapolating our work in order to calculate a somewhat meaningful value for the rate of trap-mediated recombination required in a perovskite cell that would be stable against halide segregation. In the main text we fit a linear relation between fraction of trap-mediated recombination and the value of g, extrapolating to the origin as no halide segregation is assumed when there is no charge carrier trapping within the films. Using this linear fit of gradient $1.5 \times 10^{-23}\,\mathrm{cm}^3$ we then extract a trap-mediated recombination fraction of 6.70×10^{-4} corresponding to the required value of g of $1.01 \times 10^{-26}\,\mathrm{cm}^3$ to prevent significant segregation in a film.

Charge carrier extraction is a process inherent in electricity generation and provides a competing process to that of charge carrier recombination, thus lowering the fraction of charge carriers that undergo trap-mediated recombination and stabilising the perovskite film against halide segregation. To account for charge carrier extraction here, we use a simple model proposed by Lin *et al.*[S13] that integrates an extraction rate into Equation S2; the third-order charge carrier recombination rate equation discussed in Section S6:

$$\frac{\mathrm{d}n}{\mathrm{d}t} = G(t) - k_1 n - k_2 n^2 - k_3 n^3 - c_{ext} n \tag{13}$$

Here n is the charge carrier density, t is time, $G(t)$ is the generation rate of charge carriers, k_1, k_2 and k_3 are the trap-mediated (monomolecular), band-to-band (bimolecular) and Auger recombination rate constants respectively, and c_{ext} is the charge carrier extraction rate. Under continuous illumination the charge carrier density in the perovskite film quickly reaches equilibrium, and so Equation S13 can be set equal to zero. By inputting the values of $G(t)$, k_1, k_2, k_3 and c_{ext} into Equation S13 when equal to zero it is possible to determine the fraction of charge carriers that recombine through trap states at equilibrium, $\frac{k_1 n}{G}$.

Conversely, by inputting the values of $G(t)$, k_2, k_3, c_{ext} and a required $\frac{k_1 n}{G}$, it is possible to determine the value of k_1 that will induce that fraction of trap-mediated recombination. Taking a constant value of $G(t)$ equal to $3.05 \times 10^{21}\,\mathrm{cm^{-3}\,s^{-1}}$ as discussed in this section and Section S3, k_2 to be $6 \times 10^{-10}\,\mathrm{cm^3\,s^{-1}}$ as determined from our samples (see Section S8), k_3 to be $1 \times 10^{-28}\,\mathrm{cm^6\,s^{-1}}$ in accordance with similar perovskites,[S11] c_{ext} to be $10^8\,\mathrm{s^{-1}}$ as suggested by Lin *et al.*,[S13] and the required trap-mediated recombination fraction to be 6.70×10^{-4} as determined above, we find that a k_1 value of $0.671 \times 10^{-5}\,\mathrm{s^{-1}}$ to be just sufficient to prevent halide segregation in a working $MAPb(Br_{0.5}I_{0.5})_3$ perovskite solar cell.

References

(S1) Huang, F.; Dkhissi, Y.; Huang, W.; Xiao, M.; Benesperi, I.; Rubanov, S.; Zhu, Y.; Lin, X.; Jiang, L.; Zhou, Y. et al. Gas-Assisted Preparation of Lead Iodide Perovskite Films Consisting of a Monolayer of Single Crystalline Grains for High Efficiency Planar Solar Cells. *Nano Energy* **2014**, *10*, 10–18.

(S2) NREL, Reference Solar Spectral Irradiance: Air Mass 1.5. 2004; `https://rredc.nrel.gov/solar/spectra/am1.5/`, [Online; accessed 3-November-2017].

(S3) Hoke, E. T.; Slotcavage, D. J.; Dohner, E. R.; Bowring, A. R.; Karunadasa, H. I.; McGehee, M. D. Reversible Photo-Induced Trap Formation in Mixed-Halide Hybrid Perovskites for Photovoltaics. *Chem. Sci.* **2015**, *6*, 613–617.

(S4) Crothers, T. W.; Milot, R. L.; Patel, J. B.; Parrott, E. S.; Schlipf, J.; Muller-Buschbaum, P.; Johnston, M. B.; Herz, L. M. Photon Reabsorption Masks Intrinsic Bimolecular Charge-Carrier Recombination in $CH_3NH_3PbI_3$ Perovskite. *Nano Lett.* **2017**, *17*, 5782–5789.

(S5) Draguta, S.; Sharia, O.; Yoon, S. J.; Brennan, M. C.; Morozov, Y. V.; Manser, J. M.; Kamat, P. V.; Schneider, W. F.; Kuno, M. Rationalizing the Light-Induced Phase

Separation of Mixed Halide Organic–Inorganic Perovskites. *Nat. Commun.* **2017**, *8*, 200.

(S6) Nelson, J. *The Physics of Solar Cells*; Imperial College Press, 2003.

(S7) Einstein, A. Zur Quantentheorie der Strahlung. *Phys. Z.* **1917**, *18*, 121–128.

(S8) Shockley, W.; Read Jr, W. Statistics of the Recombinations of Holes and Electrons. *Phys. Rev.* **1952**, *87*, 835.

(S9) Hall, R. N. Electron-Hole Recombination in Germanium. *Phys. Rev.* **1952**, *87*, 387.

(S10) Yang, X.; Yan, X.; Wang, W.; Zhu, X.; Li, H.; Ma, W.; Sheng, C. Light Induced Metastable Modification of Optical Properties in $CH_3NH_3PbI_{3-x}Br_x$ Perovskite Films: Two-Step Mechanism. *Org. Electron.* **2016**, *34*, 79–83.

(S11) Johnston, M. B.; Herz, L. M. Hybrid Perovskites for Photovoltaics: Charge-Carrier Recombination, Diffusion, and Radiative Efficiencies. *Acc. Chem. Res.* **2015**, *49*, 146–154.

(S12) Rehman, W.; Milot, R. L.; Eperon, G. E.; Wehrenfennig, C.; Boland, J. L.; Snaith, H. J.; Johnston, M. B.; Herz, L. M. Charge-Carrier Dynamics and Mobilities in Formamidinium Lead Mixed-Halide Perovskites. *Adv. Mater.* **2015**, *27*, 7938–7944.

(S13) Lin, Q.; Wang, Z.; Snaith, H. J.; Johnston, M. B.; Herz, L. M. Hybrid Perovskites: Prospects for Concentrator Solar Cells. *Adv. Sci.* **2018**, *5*, 1700792.